ELECTROMAGNETICALLY COUPLED PATCH ANTENNA ARRAY

by

Squadron Leader Amit Belapurkar

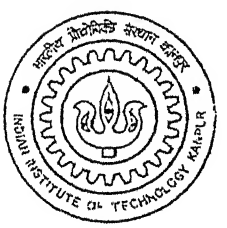

to the

DEPARTMENT OF ELECTRICAL ENGINEERING

INDIAN INSTITUTE OF TECHNOLOGY, KANPUR

February 1999

ELECTROMAGNETICALLY COUPLED PATCH ANTENNA ARRAY

A Thesis Submitted

in Partial Fulfillment of the Requirements

for the Degree of

Master of Technology

by

Squadron Leader Amit Belapurkar

to the

DEPARTMENT OF ELECTRICAL ENGINEERING

INDIAN INSTITUTE OF TECHNOLOGY, KANPUR

February 1999

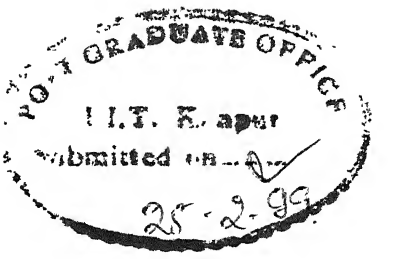

Certificate

It is certified that the work contained in the thesis entitled " ELECTROMAGNETICALLY COUPLED PATCH ANTENNA ARRAY", by *Squadron Leader Amit Belapurkar*, has been carried out under my supervision and that this work has not been submitted elsewhere for a degree.

February 1999

Dr. M. Sachidananda
Professor
Department of Electrical Engineering
I.I.T Kanpur

Abstract

The microstrip antennas have notable advantages as compared to the conventional microwave antennas. The light weight, small volume and low planar configuration of the microstrip antennas has made them very popular. Narrow bandwidth is however the most significant disadvantage of the microstrip antenna. The bandwidth increases considerably by using a thicker substrate, this however increases the mutual coupling.

In order to utilize the larger bandwidth of the thicker substrate but at the same time reduce the mutual coupling EM coupled rectangular patch antenna is proposed in this study. In this the patch radiator is kept over the microstrip line and the coupling between the patch antenna and the microstrip line takes place electromagnetically.

To test the design of the EM coupled patch antenna and its suitability for array application it was decided to make an eight element broad side array with side lobe level below 25 dB and operating at 9.25 GHz.

Acknowledgement

I wish to express my sincere gratitude to my guide Dr M. Sachidananda for his supervision, guidance and encouragement throughout this study.

I express my thanks to Dr A. Biswas who was always a source of encouragement for me. I am deeply indebted to Rajeev, Ashish and Pawan of Com Dev phase group. I take this opportunity to express my gratitude to Mr S.K. Kole of the PCB section.

I will be failing in my duty if I do not convey my gratitude to the Indian Air Force, having sent me for this course.

Lastly I will like to thank my wife Sonali and son Siddharth for their kind understanding and support without which I would not have achieved the results.

Contents

List of Figures

Chapter 1

Introduction

As shown in figure 1.1, a microstrip antenna in its simplest form consists of a radiating patch on one side of a dielectric substrate ($\epsilon_r \leq 10$) and ground plane on the other side. The radiating patch can assume any shape but most common shapes are rectangular and circular.

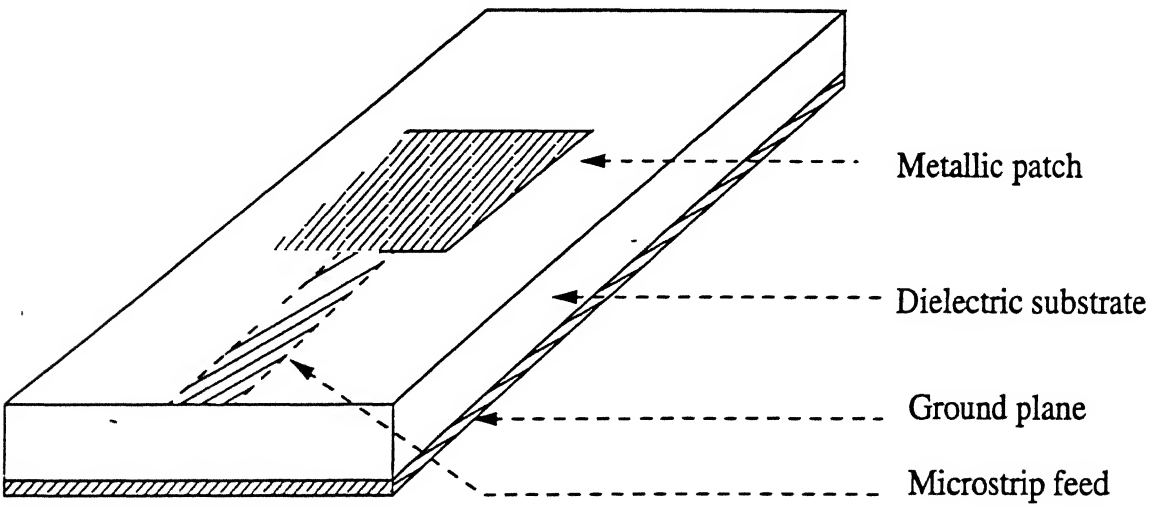

Figure 1.1: Microstrip rectangular patch antenna

The flow of electromagnetic power in the patch antenna is by the guided waves. The guided waves transport the energy along the microstrip or coaxial line to the feed point. The energy then spreads out into the region under the patch; some of

it crosses the boundary of the patch, to be radiated in to space. In practice, the permittivity of the dielectric layer is small and its thickness is small, so the region under the patch behaves like a parallel plate transmission line. Waves that leave the feed point see almost an open circuit when they arrive at the perimeter of the patch and considerable reflection occurs, so that the fraction of incident energy emerging to be radiated is small. This suggests that the patch behaves more like a cavity than a radiator, and pin points its principle disadvantages that it is a low power antenna having a narrow band width.

Microstrip antennas have several advantages as compared to conventional microwave antennas. They are light in weight, have small volume and have low profile planar configuration. They can be made conformal and hence do not perturb the aerodynamics of aerospace vehicles. Due to this they can be easily mounted on missiles, rockets and satellites. Linear and circular polarizations are possible with simple changes in feed positions. Microstrip antennas are compatible with microwave integrated circuits and hence solid state devices can be fabricated on the antenna substrate itself. Multiple frequency microstrip antennas can be easily designed. Feed lines and matching networks can be simultaneously fabricated with the antenna structure.

Microstrip antennas also have some disadvantages compared to conventional microwave antennas. They have narrow bandwidth and have a low power handling capacity. Surface waves may be excited along the antenna substrate, resulting in radiation in undesired directions. These surface waves produce excessive mutual coupling between the antenna array elements.

Due to the notable advantages of microstrip antennas over the conventional antennas, microstrip antennas have been developed for several applications like satellite communications, Doppler radar, missile telemetry, phased array antennas etc.

The concept of microstrip radiators was first proposed by Deschamps [1] as early as 1953. The first practical antennas were developed in the early 1970's by Howell [2] and Munson [3]. Since then, extensive research and development of microstrip antennas and arrays, exploiting the numerous advantages. have led to diversified ap-

plications and to the establishment of the topic as a separate entity within the broad field of microwave antennas. Mathematical modeling of the basic microstrip radiator was initially carried out by the application of transmission line analogy to simple rectangular patches fed at center of a radiating wall [3,4]. In this technique, the patch is modeled as a transmission line with no transverse field variation. The radiating edges are considered as narrow slots radiating in to half space. The effective length of the rectangle, after taking in to account the open end fringing fields is chosen equal to half a wavelength $(\lambda_o/2\sqrt{(\epsilon_{eff})})$, here ϵ_{eff} is the effective dielectric constant, which makes the two parallel radiating slots to be excited with equal and opposite voltages. The slot admittance, input impedance and resonant frequency are evaluated from the slot width and the effective dimensions of the patch. The main disadvantage of this model is that this model cannot be applied for geometries other than rectangles. The first mathematical analysis of a wide variety of microstrip patch shapes was carried out by Lo *et al.* [5,6,7]. This model has successfully explained the properties of microstrip antennas for various configurations. This method models the antenna as a cavity with magnetic walls along the edge of the metallic patch. The input impedance is calculated by considering the different modes that can exist in a cavity. The present thesis is based on this model.

Narrow bandwidth is the most significant disadvantage of the microstrip antennas. Several methods have been employed to increase the bandwidth. The bandwidth of the microstrip antennas can be increased by using trapezoidal structures instead of commonly employed rectangular structure. The bandwidth of the antenna can be increased by coupling short circuit quarter wavelength parasitic elements to the radiating edges of the rectangular patch antenna and by placing parasitic strips parallel to the non radiating edges of square patch antenna [8]. The bandwidth of the microstrip antennas can be increased many times by employing multi-fed microstrip antenna arrays in log-periodic and semi log-periodic configurations [9]. The bandwidth of the microstrip antenna can be increased by using thicker dielectric substrate however this increases the surface wave propagation. In microstrip antennas, in addition to radiation, surface waves may be excited giving rise to end fire radiation, and hence must be

considered in the design. These waves are TM and TE modes which propagate into the substrate outside the microstrip patch. The modes are characterized by waves attenuating in the transverse direction (normal to the antenna plane) and having a real wave number in the direction of propagation. The phase velocity of the surface waves is strongly dependent on the dielectric constant , ϵ_r, and thickness ,h, of the substrate. The surface waves will give rise to mutual coupling between the elements of antenna array. The mutual coupling affects the radiation pattern of the array and has to kept minimum. The mutual coupling becomes more critical in the phased array antennas as it changes with the scanning angle. The mutual coupling is also a function of frequency.

In order to utilize the larger bandwidth of the thicker substrate but at the same time reduce the mutual coupling electromagnetically coupled patch antenna is proposed in the study. In this the patch radiator is placed above the microstrip line and the coupling occurs due to interaction of the fringe fields. The excess dielectric is removed everywhere except just under the metallic patch. This antenna is then excited electromagnetically by a microstrip line fed in the center as shown in figure 2.1.

The thesis is organized in five chapters. Chapter 2 deals with the design of the EM coupled microstrip antenna. EM coupled antenna differs from the cavity model discussed by Lo *et al.* due to the presence of air dielectric discontinuity. Resonant frequency and input impedance was measured for the EM coupled patch antenna and modifications were made to the existing formulas. Thus design curves and equations were formulated for the EM coupled microstrip patch antenna. Chapter 3 deals with the linear array design. As a test of the theory developed in Chapter 2 an eight element linear array was designed and fabricated. Measurements were carried out on this antenna and results were compared with the theoretical calculations. Chapter 4 gives the conclusion and scope for further work.

Chapter 2

Study Of EM Coupled Patch Antenna

2.1 Description of the antenna

The antenna proposed in this study is an EM coupled rectangular patch antenna. In this the patch radiator is kept over the microstrip line and the coupling between the patch antenna and the microstrip line takes place electromagnetically.

The antenna consists of a rectangular dielectric patch (one side copper coated) placed symmetrically on a microstrip line. This microstrip line is printed on a copper clad dielectric substrate of the same material as shown in figure 2.1.

To achieve minimum radiation losses from the microstrip line it is necessary to keep h_2 small, this also ensures that the microstrip width is not very large. However to achieve larger bandwidth it is necessary to keep the total height h as large as possible. In the microstrip patch antenna proposed here it is possible to achieve both. In this arrangement the height h_1 can be kept small but the height h_2 can be increased.

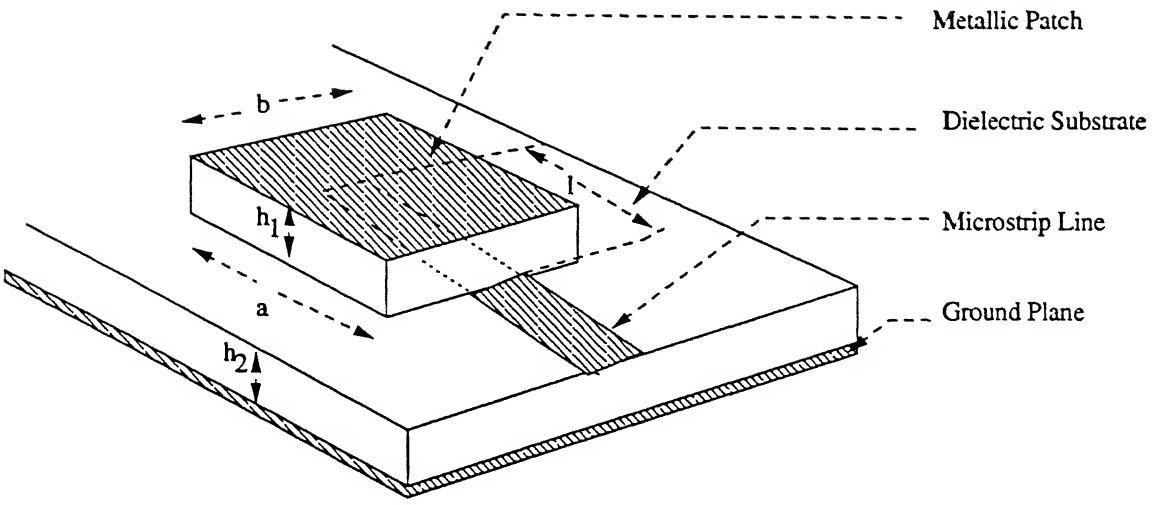

Figure 2.1: The EM coupled rectangular patch antenna

Here,

a = length of the rectangular patch.

b = width of the rectangular patch.

h_1 and h_2 are the height of the substrate.

$h_1 + h_2 = h$.

l = length of open circuited stub line feeding the patch antenna.

ϵ_{r1} and ϵ_{r2} are the dielectric constant for height h_1 andh_2.

In the EM coupled rectangular patch antenna proposed in the study the rectangular patch antenna of length a, width b and height h_1 is fabricated separately. This is then placed symmetrically about a microstrip line printed on a substrate of height h_2.

The arrangement here provides the flexibility of choosing different h_1 and h_2 with dielectric constant ϵ_{r1} and ϵ_{r2} respectively, however in this study ϵ_{r1} and ϵ_{r2} are taken to be equal.

2.2 The cavity model of the patch antenna

Lo *et al.* [6] proposed a model for treating microstrip antennas as cavities in microstrip lines. Refer to figure 2.2. The model is based on the following assumptions:

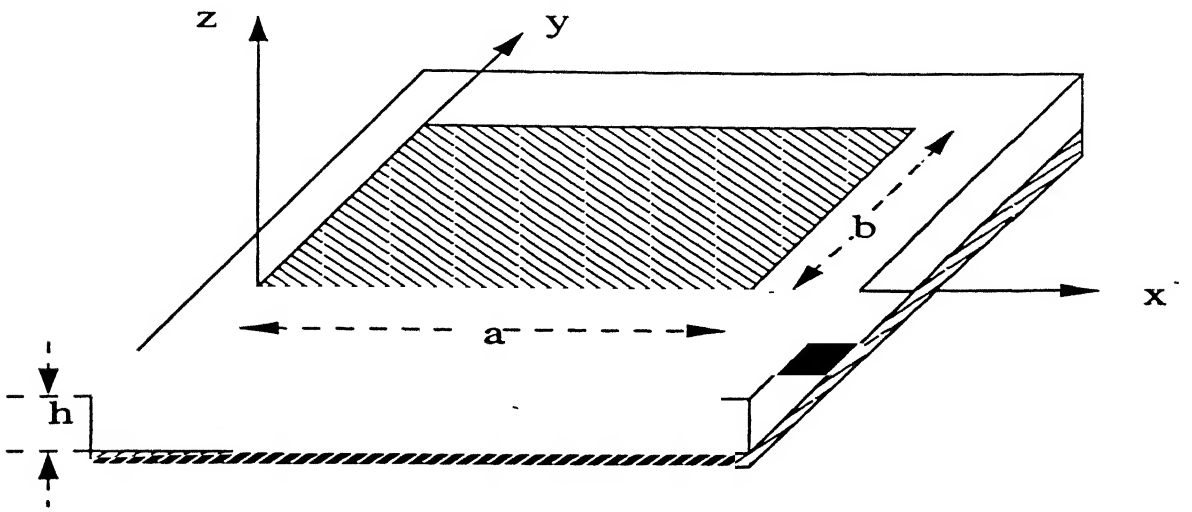

Figure 2.2: The cavity model

- Only the z component of the electric field, $\overline{E}$, and the x and y components of the magnetic field , $\overline{H}$, exists in the region bounded by the microstrip and the ground plane.
- The field in the region mentioned above is independent of the z coordinate for all frequencies.
- The electric current in the microstrip has no components normal to the edge at any point on the edge, which implies that the tangential component of $\overline{H}$ along the edge is negligible.

The region between the microstrip and the ground plane may be treated as a cavity bounded by magnetic wall along the edge, and by electric walls from top and bottom. The fields in the antenna may be assumed to be those of the cavity, hence the radiation pattern, radiated power and input admittance at any feed point may

be evaluated. EM coupled patch antenna differs from the above model due to the presence of air-dielectric discontinuity. The main disadvantage of the cavity model is that it is an approximate model. Since the structure being analyses has a discontinuity it is difficult to carry out full wave rigorous analysis. The present approach has been to modify the available design equations for resonant frequency [10] and those available for input impedance calculation [11] . The modification has been carried out by carrying out measurements on the rectangular patch antenna.

The lowest resonant frequency,f, of the rectangular patch along the x-axis occurs when the length is a half wavelength, that is

$$f = \frac{1}{2a\sqrt{\epsilon\mu}}$$

The fringing fields at the ends of the line resonator represent an extension of the element, making the physical length shorter than the effective one. The additional length, Δl, for an open circuited microstrip line is given in the literature [10].

$$\Delta l = 0.412h\left(\frac{\epsilon_{eff}+.3}{\epsilon_{eff}-.258}\right)\left(\frac{b/h+.262}{b/h+.813}\right)$$

b is the breadth of the patch, h is the height of the patch. The effective dielectric constant ϵ_{eff} is given by

$$\epsilon_{eff} = \left(\frac{\epsilon_r+1}{2}\right) + \left(\frac{\epsilon_r-1}{2}\right)\left(1+\frac{12h}{b}\right)^{-1/2}$$

Analysis of the rectangular patch antenna is simplified by regarding the patch as a microstrip line resonator, where the radiation is regarded as being due to the ends of the line acting as open-circuit line radiators. The analysis has to take into account the effects of mutual coupling between the end radiators in the present configuration. The transmission line model is shown in the figure 2.3.

The feed point P may represent either a microstrip transmission line coupled to the edge of the patch antenna, or a coaxial line passing through the substrate. The susceptance B is representative of the effects of the fringing fields at the end of the line, and could be represented as an effective line length extension Δl.

The self-conductance G_r is given as :

1. $G_r = w^2/90\lambda_o^2, \qquad w < 0.35\lambda_o$

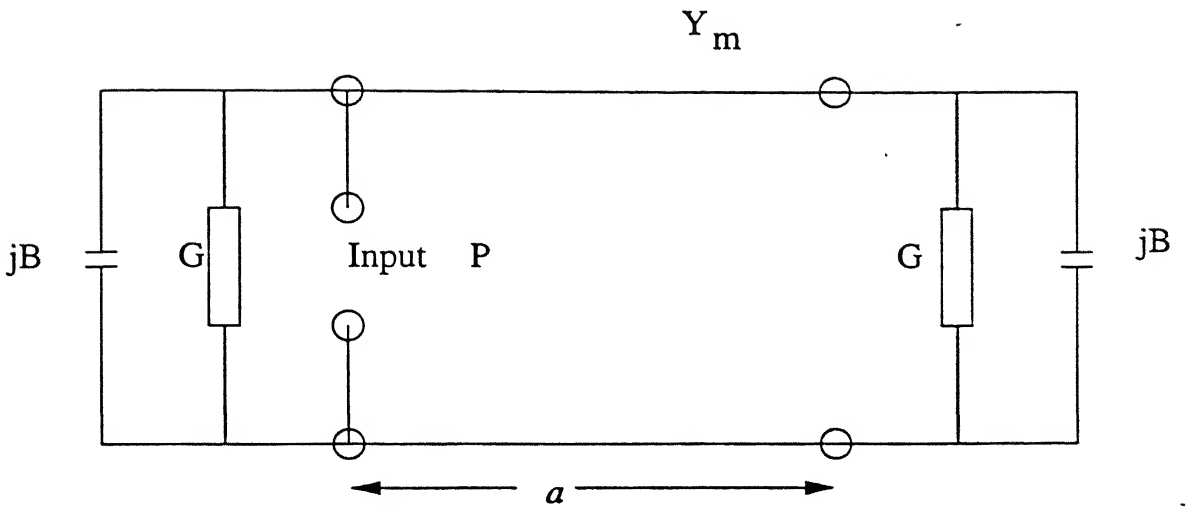

Figure 2.3: Transmission line model of rectangular patch antenna

2. $G_r = w/120\lambda_o - 1/60\pi^2, \qquad .35\lambda_o \leq w \leq 2\lambda_o$

3. $G_r = w/120\lambda_o, \qquad 2\lambda_o < w$

Here λ_o is free space wavelength and w is effective conductor width.

The mutual conductance G_m between the ends may be determined by integrating the interference component of the far-field radiation patterns of two magnetic current sources of length w spaced by a length a perpendicular to their length.

$$G_m = \frac{1}{120\pi^2} \int_0^{\pi} \frac{sin^2\left(\frac{\pi w cos\theta}{\lambda_o}\right)}{cos^2\theta} sin^3\theta J_o\left(\frac{2\pi a sin\theta}{\lambda_o}\right) d\theta$$

If the total admittance at each radiating end of the line is G + jB, which includes both self and mutual impedances, and the microstrip transmission line admittance is Y_m , then at resonance the input impedance is given by Derneryd [11].

$$Z_{in} = \frac{0.5}{G_r + G_m}$$

2.3 Calibration of NA and measurement of S_{11}

At microwave frequencies, systematic effects such as leakage, test port mismatch and frequency response will affect the measured data. However in a stable environment these effects are repeatable and can be measured by the network analyzer. This process

is called "Measurement Calibration". During measurement calibration, a series of known devices (standards) are connected. The systematic effects are determined as the difference between the measured and known response of the standards. The process of mathematically removing these errors is called "Error Correction".

In the case of the conventional automatic network analyzer (ANA), which is based upon the four-port reflectometer, it is convenient to visualize the calibration as shown in the figure 2.5. Here the non-ideal reflectometer has been modeled by an ideal one

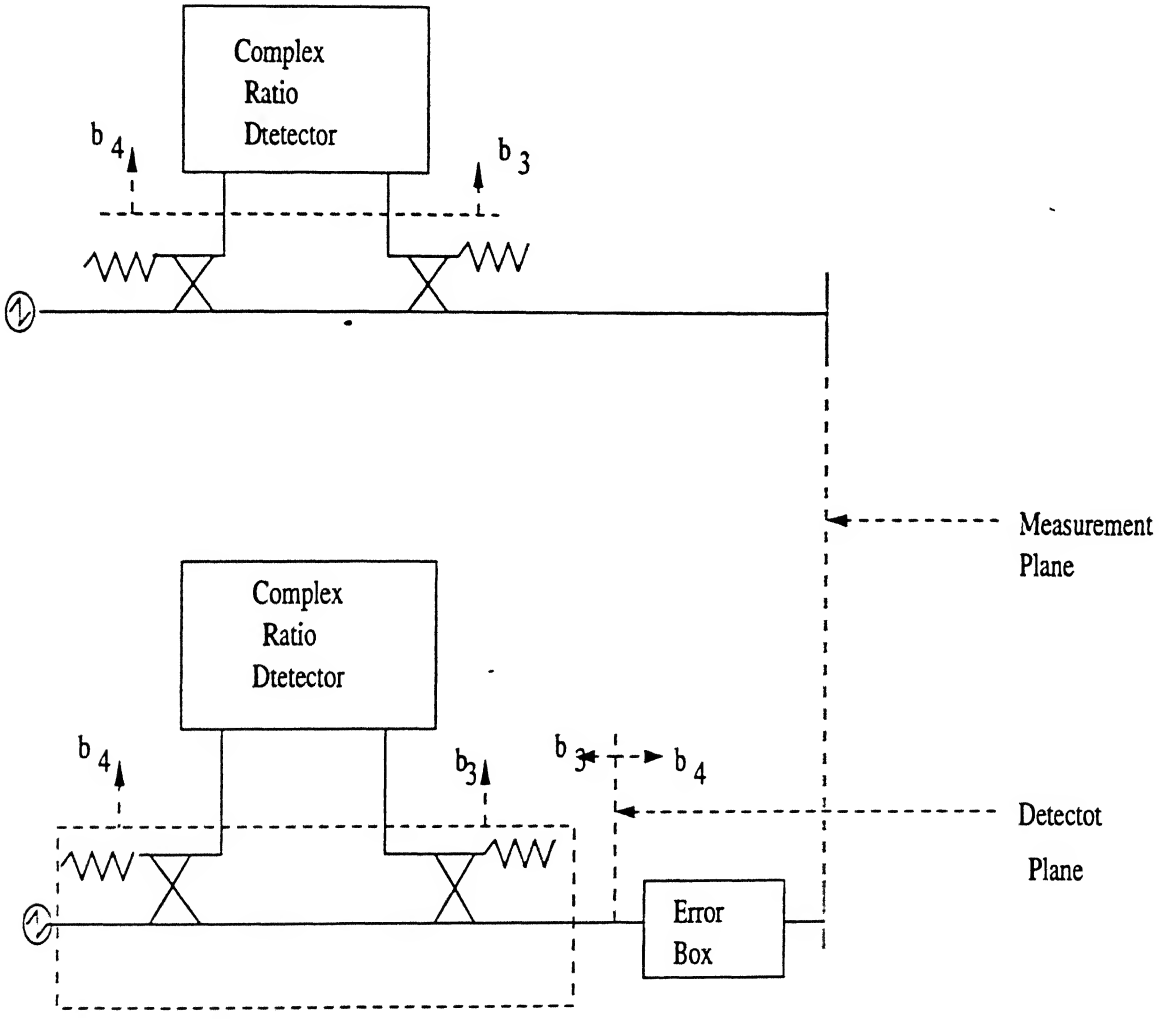

Figure 2.4: Reflectometer model

in cascade with a 2-Port 'error box.' The properties of the ideal reflectometer can be chosen in such a way that its side arm wave amplitudes b_3, b_4 are , respectively,

equal to the emergent and incident waves at a fictitious 'detector plane' which is the input to the 2-Port 'error box.' The parameters of the 'error box' are provided by the ANA calibration. after this has been done, these parameters, in combination with the reading of the complex ratio detector, permit an exact determination of the signals at the measurement plane. In order to make 2-Port measurements, it is convenient to introduce a second (non-ideal) reflectometer and complex ratio detector which is then modeled in the same way as the first one. This is shown in figure 2.6. The calibration requirement now calls for obtaining the parameters of error boxes A and B.

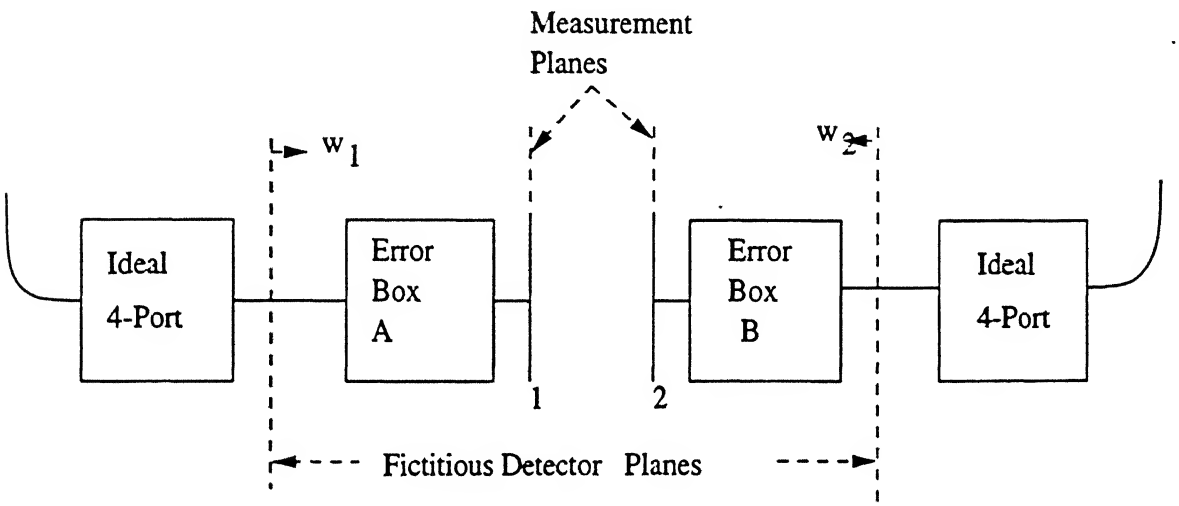

Figure 2.5: Two port measurements

THRU-REFLECT-LINE (TRL) [12] is an approach to 2-Port calibration that relies on transmission lines rather than a set of discrete impedance standards. Although its mathematical derivation is different than the conventional FULL 2-PORT, application of the technique results in the same 12-term error correction model. There are three key advantages gained when using transmission lines as reference standards:

- Transmission lines, which are used as standards in the TRL approach are easy to realize, as compared to the precision coaxial standards used for 2-PORT calibration.

- The impedance of transmission lines can be accurately determined from phys-

ical dimensions and materials. Software like PUFF are available to calculate impedance of the transmission line depending on the dimensions and material.

- Transmission lines have been traditionally used as standards and are well understood.

TRL refers to three basic steps in the calibration process. THRU means connection of port 1 and port 2, directly or with a short length of transmission line. REFLECT means to connect one-port high reflection coefficient devices to each port. LINE means to insert a short length of transmission line between port 1 and port 2. Given the scattering parameters of these three 2-Ports, it is possible to solve for the individual scattering parameters of error two ports A and B.

The steps of the TRL calibration method are shown in figure 2.7. The calibration plane is established as the plane where the fixture halves meet. A zero length

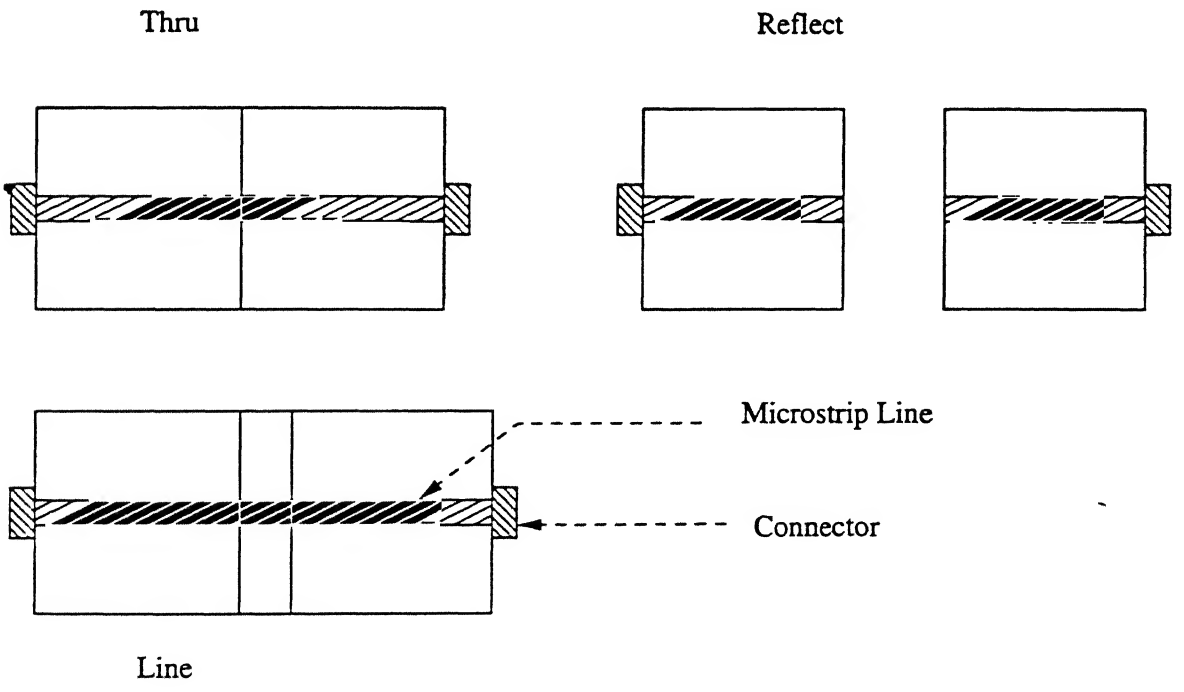

Figure 2.6: Calibration standards

THRU is achieved connecting the two halves of the fixture together. The most simple REFLECT is an open circuit. The LINE standard is a short microstrip line inserted

between the fixture halves. To construct this standard, the physical

All the three standards were fabricated in the laboratory. It was decided to establish the calibration plane at 15 mm from the connector. A copper clad dielectric substrate made of duroid ($\epsilon_r = 2.2$) with 0.8 mm thickness was taken. A 50Ω microstrip line of length 30 mm was printed on it using the conventional photo-itching techniques. The width of the microstrip line was calculated using the software package PUFF, this is the THRU standard. Similarly a 15 mm and a 35.451 mm microstrip line was printed on a similar substrate, they are the REFLECT and LINE standards respectively. The length of LINE is calculated by adding physical length of $\lambda/4$ line at 10 GHz to the length of the THRU standard. The physical length of $\lambda/4$ line is calculated using PUFF and it comes to 5.451 mm.
The three standards were then mounted on a metallic blocks and connectors were connected to the microstrip line as shown in the figure 2.6. These three standards were used for the calibration of the network analyzer (HP 8720c). This network analyzer calculates and stores the 'Error matrix'. For any measurements performed on the network analyzer this 'Error matrix' is removed and the corrected results are given.

To fabricate the rectangular patch antenna a copper clad dielectric substrate made of duroid ($\epsilon_r = 2.2$) with $h_1 = 0.8$ mm was taken. A 50Ω microstrip line was printed using the software package PUFF. This was then mounted on a metallic block and to one end of the microstrip line a connector was attached. Another copper clad dielectric substrate made of the same material and of some definite thickness, h_2, was taken. Rectangular blocks of required dimensions were printed on this substrate using the photo-etching technique. These rectangular blocks were then cut in the laboratory and placed on the microstrip line such that the microstrip line feeds at the center of the block as shown in figure 2.1.

The setup for measuring S_{11} is shown in the figure 2.7. The S_{11} is now measured at the calibration plane which is 15 mm from the connector. The rectangular patch had to be moved on the microstrip line to achieve the best match. The rectangular patch thus was not necessarily at the calibration plane and the measured S_{11} had to

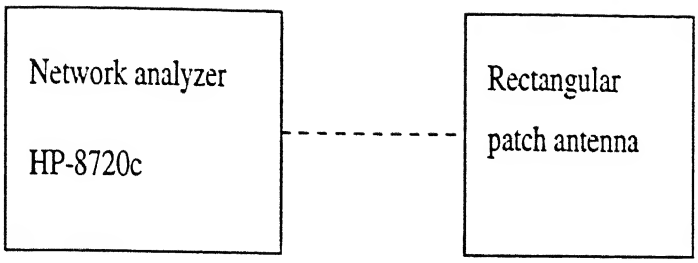

Figure 2.7: Setup for measuring S11

be corrected to get the S_{11} at the plane where patch was positioned. As it is known that the change in the reference plane does not change the magnitude of S_{11} and the correction was done in the measured S_{11} by multiplying it by $e^{2j\beta l_1}$. Here β is the propagation constant in the dielectric substrate of height h_2 and l_1 is the shift in the positioning of the rectangular patch from the calibration plane.

S_{11} is the most important measurement as it is used to calculate the input impedance. The input impedance, Z'_{in} , is given by :

$$Z'_{in} = \frac{1+S_{11}}{1-S_{11}}$$

2.4 Results and discussions

As discussed earlier the approach in the thesis has been to modify the design equations available for the directly coupled antenna. Number of measurements were carried out on the rectangular microstrip EM coupled patch antenna to formulate design equations and design curves. The aim was to develop an EM coupled rectangular patch antenna operating in the X-band. Design equations available for the directly coupled rectangular microstrip antenna were taken as the guideline for selection of patch antenna dimensions. The dimensions were chosen so that the antenna operates in the X-band. ϵ_{r1} and ϵ_{r2} were kept equal to 2.2. Three set of rectangular patch antennas were fabricated using the method described above.

- In the first set h_1 was chosen to be 0.8mm. Width , b , was taken as 1.22 cm and length ,a, was varied from 0.82 cm to 1.23 cm. Eight rectangular patch antennas

were thus fabricated.

- In the second set h_1 was chosen to be 1.6mm. Width , b , was taken as 1.40 cm and length ,a, was varied from 0.79 cm to 1.21 cm. Eight rectangular patch antennas were thus fabricated.

- In the third set h_1 was chosen to be 0.8mm. Length , a , was taken as 1.00 cm and width ,b, was varied from 0.50 cm to 1.27 cm. Eight rectangular patch antennas were thus fabricated.

The most important important measurement carried out on the rectangular patch antenna is the measurement of complex reflection coefficient S_{11}. The measurements were carried out on network analyzer (HP 8720c). The input impedance was calculated from S_{11}. The rectangular patch antenna was placed at the center of the feed line and the stub insertion length ,l, is varied to achieve the match. This is shown by maximum dip in the magnitude S_{11} vs frequency plot in the network analyzer. 24 set of readings were thus generated.

Input impedance was calculated using the complex reflection coefficient S_{11}. Figures 2.8 to 2.11 show the magnitude S_{11} vs frequency characteristics for the rectangular patch antenna. It can be seen from the figure 2.8 that the minimum S_{11} of -28 dB is around 8.6 GHz, the 10 dB bandwidth is around 0.4 GHz. If figures 2.8 and 2.10 are compared it can be seen that the minimum S_{11} of -23 dB is around 8.8 GHz, the 10 dB bandwidth is around 1 GHz in figure 2.10. This shows that the a much greater bandwidth is obtained if larger value of h_1 is taken. However a better match is obtained when h_1 is taken equal to h_2.

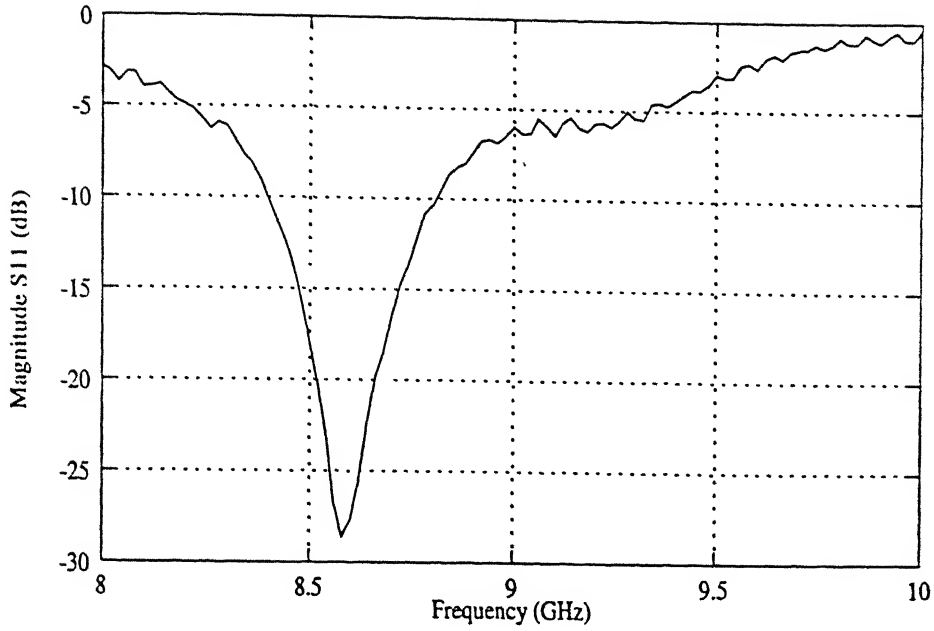

Figure 2.8: Magnitude S11 vs frequency characteristics for a patch of length 1.10cm, width 1.22cm and height 0.16cm

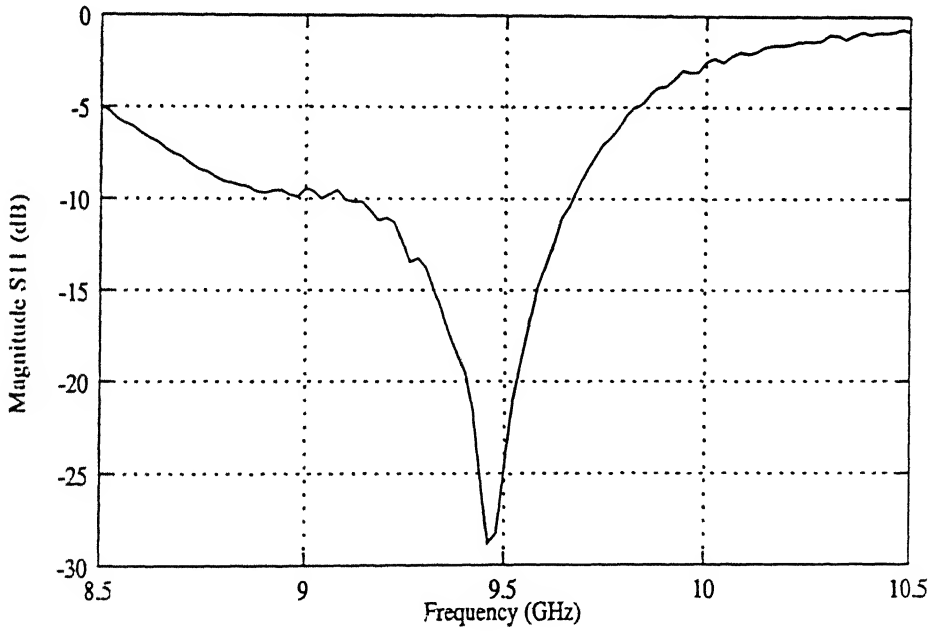

Figure 2.9: Magnitude S11 vs frequency characteristics for a patch of length 1.04cm, width 1.22cm and height 0.16cm

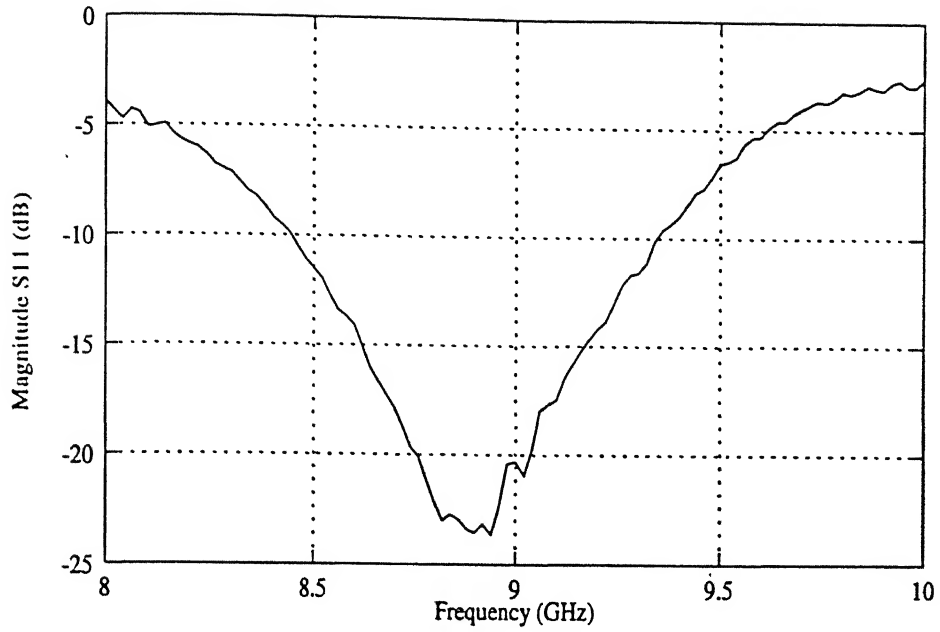

Figure 2.10: Magnitude S11 vs frequency characteristics for a patch of length 1.02cm, width 1.40cm and height 0.24cm

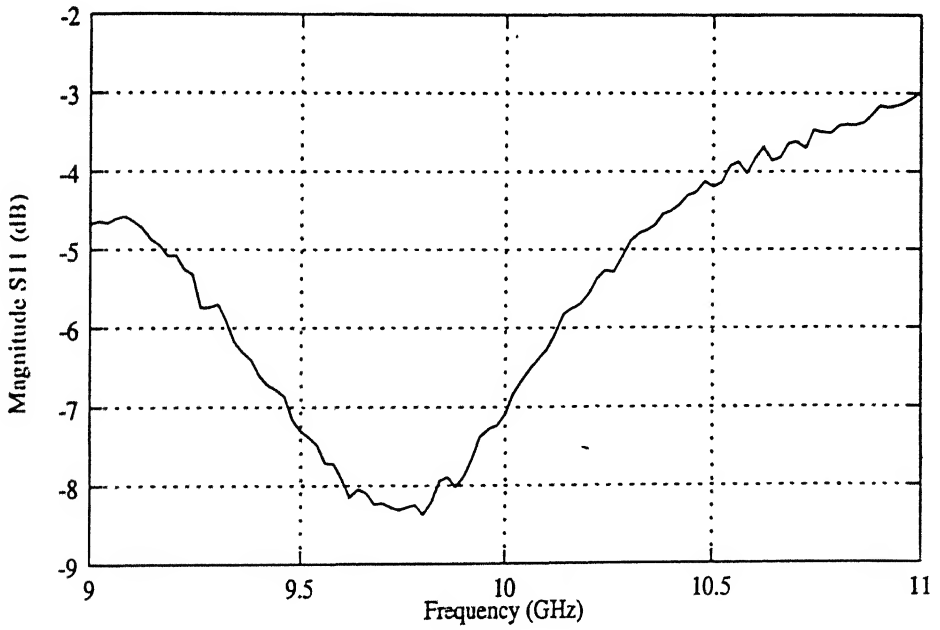

Figure 2.11: Magnitude S11 vs frequency characteristics for a patch of length .912cm, width 1.40cm and height 0.24cm

Figures 2.12 to 2.16 show the variation of input impedance with frequency for various patch dimensions. In the figures the dotted line represents the imaginary part of the input impedance and the solid line represents the real part of the input impedance. It can be seen from the figures that at resonance the imaginary part of the input impedance goes to zero. Another characteristics which can be observed from these graphs is that the reactance is negative before the resonant frequency and becomes positive after the resonant frequency. The radiation resistance is maximum at the resonance. ϵ_r is taken as 2.2 in all the figures.

In figure 2.12 the measured resonant frequency is 9.78 GHz and the measured input impedance at resonance is 55Ω.

In figure 2.13 the measured resonant frequency is 10.35 GHz and the measured input impedance at resonance is 90Ω.

In figure 2.14 the measured resonant frequency is 10.65 GHz and the measured input impedance at resonance is 120Ω.

In figure 2.15 the measured resonant frequency is 10.9 GHz and the measured input impedance at resonance is 200Ω.

In figure 2.16 the measured resonant frequency is 10.4 GHz and the measured input impedance at resonance is 150Ω.

Another important observation which can be made from these figures is that the rectangular patch antennas with $h_1 = .8$ mm have lower input impedance as compared to the rectangular patch antennas with $h_2 = 1.6$ mm. Input impedance was calculated from the measured S_{11} for twenty four rectangular patch antennas but only five sample graphs have been shown here.

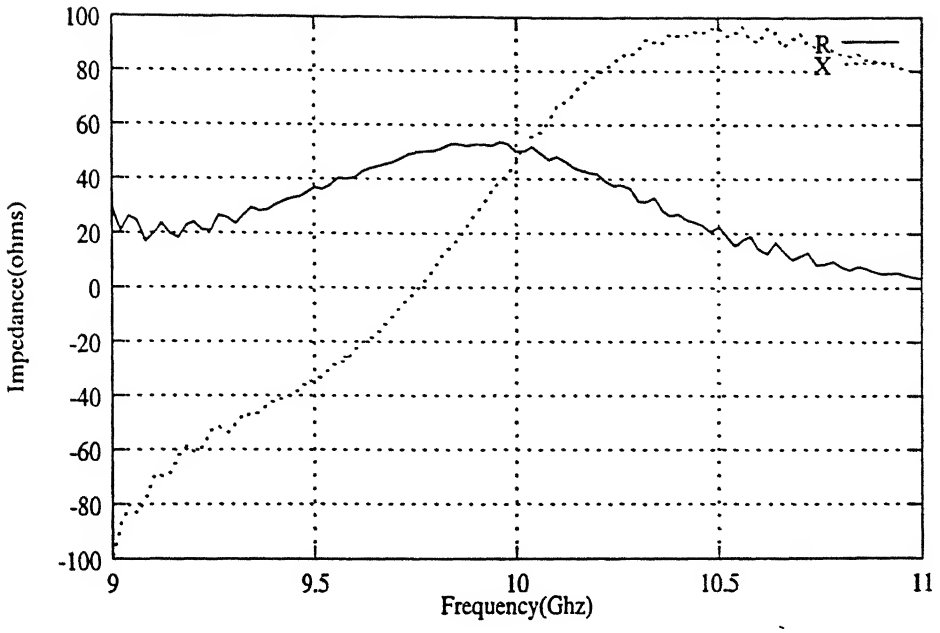

Figure 2.12: Input impedance vs frequency characteristics for a patch of length 0.97cm, width 1.22cm and height 0.16cm

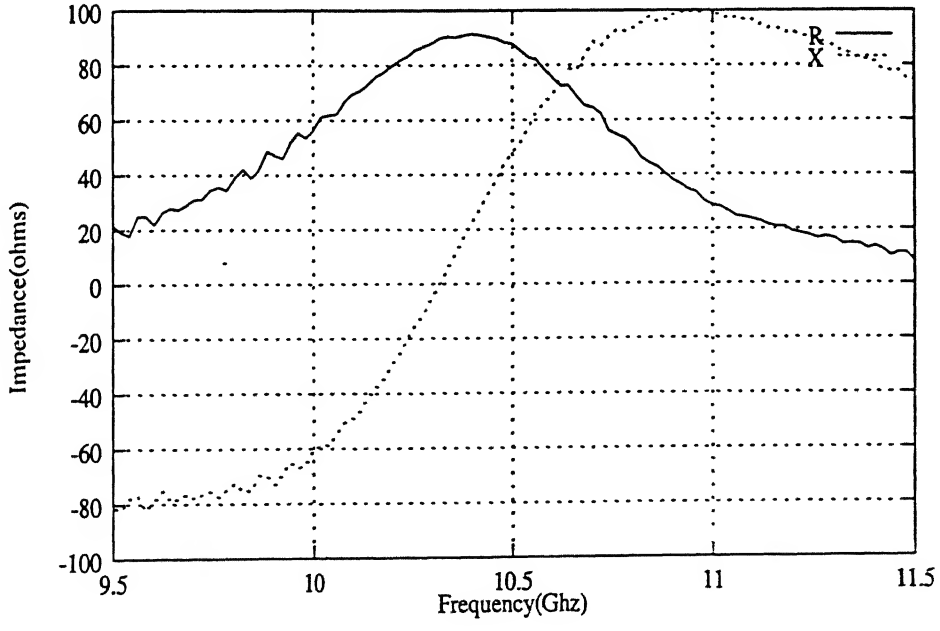

Figure 2.13: Input impedance vs frequency characteristics for a patch of length 0.92cm, width 1.22cm and height 0.16cm

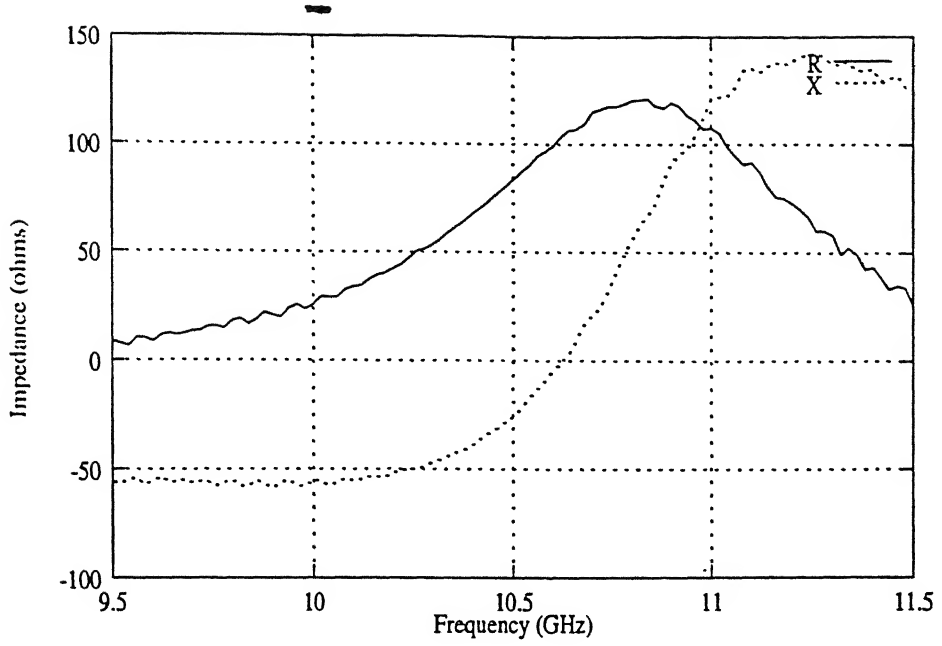

Figure 2.14: Input impedance vs frequency characteristics for a patch of length 0.89cm, width 1.22cm and height 0.16cm

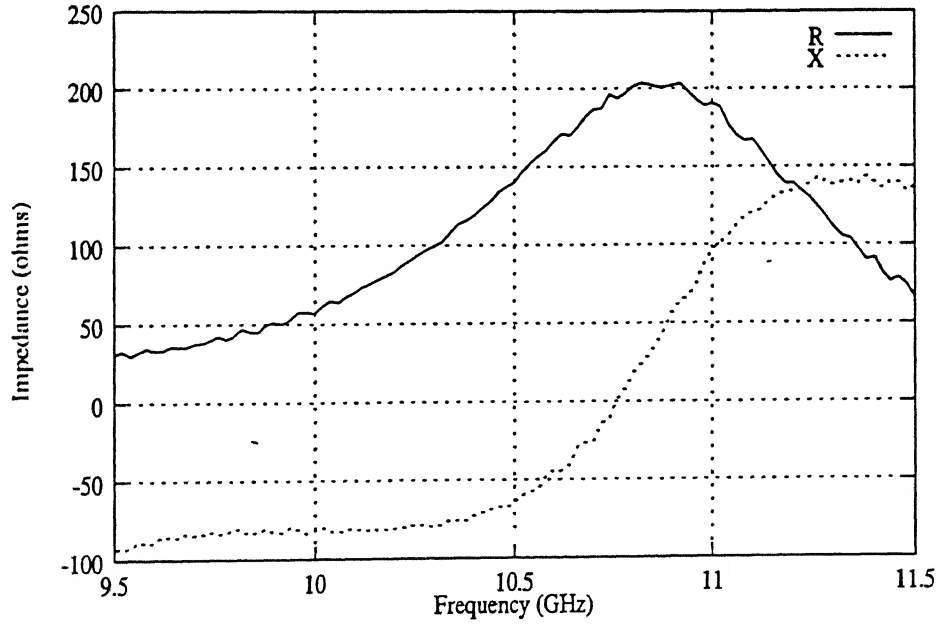

Figure 2.15: Input impedance vs frequency characteristics for a patch of length 0.828cm, width 1.40cm and height 0.24cm

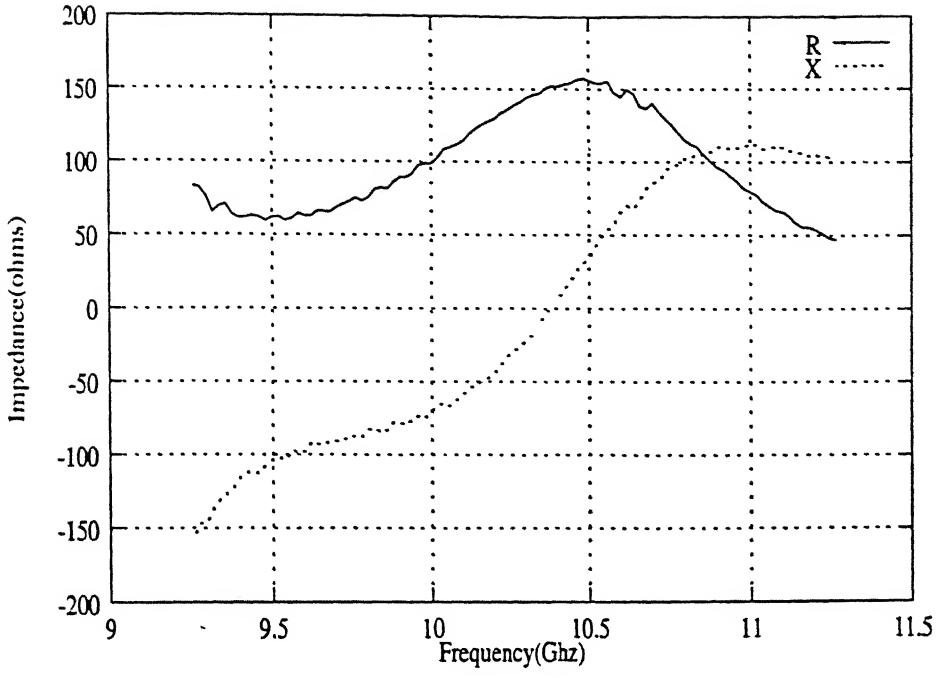

Figure 2.16: Input impedance vs frequency characteristics for a patch of length 0.874cm, width 1.40cm and height 0.24cm

Variation of resonant frequency as a function of length for a given height and width is shown in the figure 2.17. This graph was plotted using the results of set 1 and set 2 of rectangular patch antennas. This graph can be utilized to select length, a, for a given resonant frequency. The continuous line is for $h = 0.8$ mm and dotted line is for $h = 1.6$ mm. It can be seen from the graph that resonant frequency is a strong function of. a. Small variation of length ,a, results in a large variation in resonant frequency.

Variation of resonant frequency as a function of width for a given height and length is shown in the figure 2.18. This graph was plotted using the results of set 3. It can be seen from the graph that variation of width ,b, results in a very small variation in resonant frequency

The variation of radiation resistance with patch width for a given length and height is shown in the figure 2.19. This graph is plotted using the results of set 3.

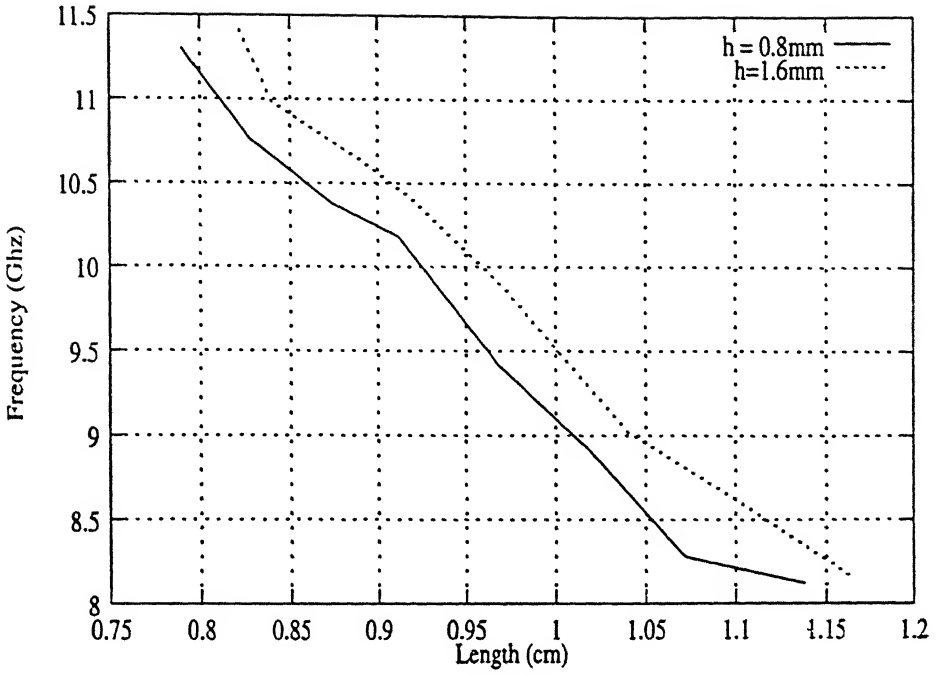

Figure 2.17: Resonant frequency vs length for a given width and height

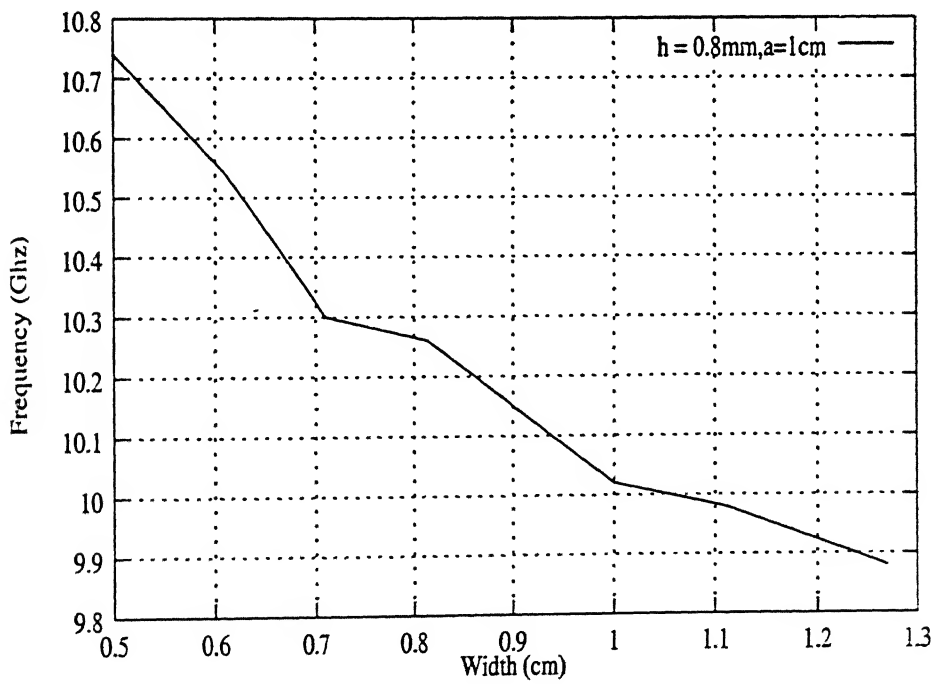

Figure 2.18: Resonant frequency vs width for a given length and height

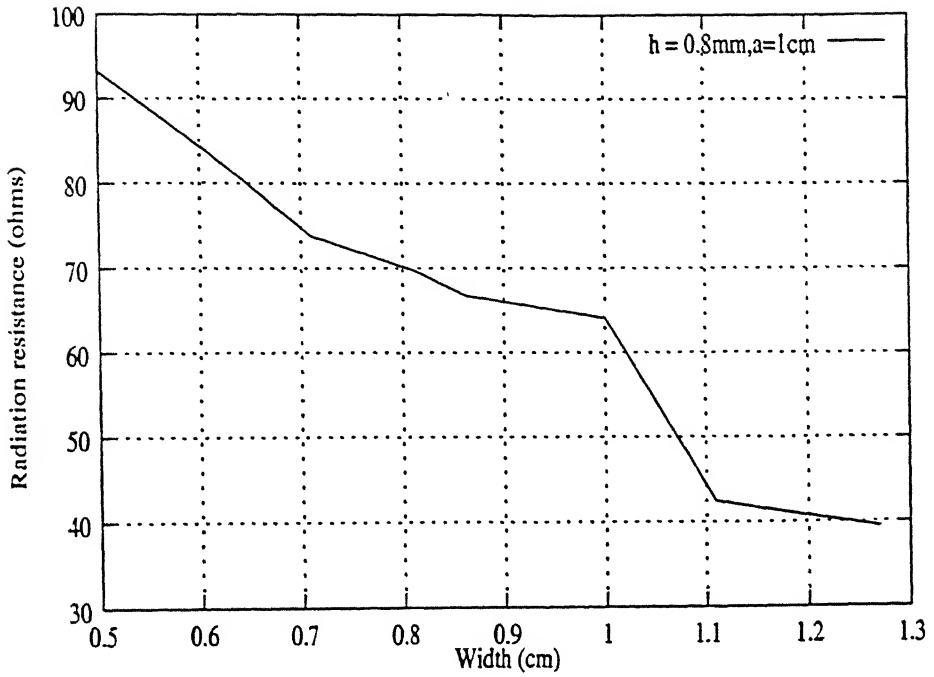

Figure 2.19: Radiation resistance vs width for a given length and height

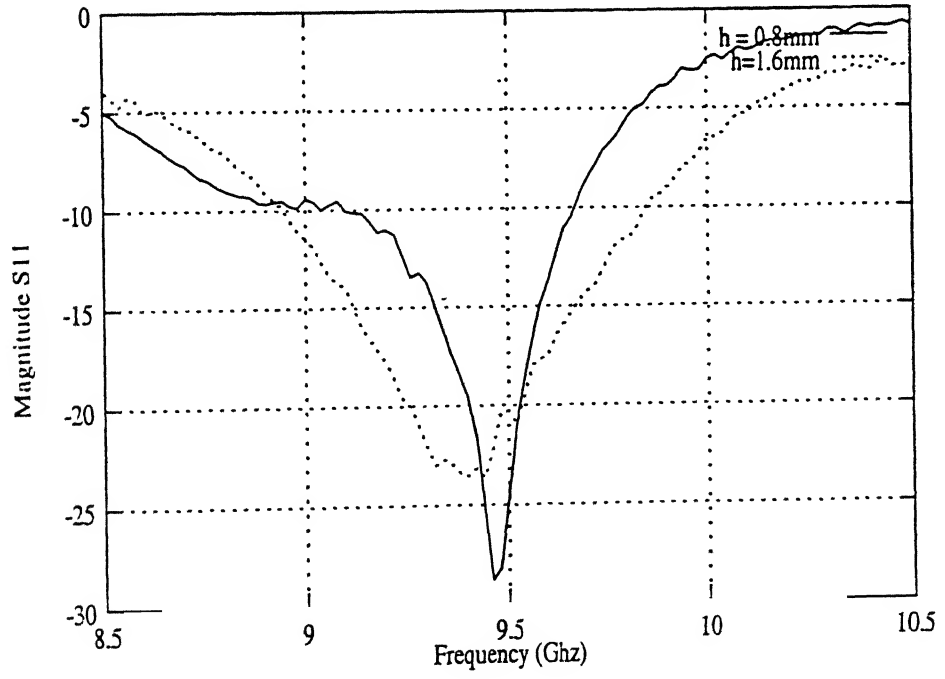

Figure 2.20: Magnitude S11 vs frequency for different thickness

It can be seen from figure 2.20 that VSWR bandwidth is a function of height , h. Here results of set 1 and set 2 were utilized. The solid curve is for $h = 0.8$mm and dotted curve is for $h = 1.6$mm . The bandwidths of these were compared and from figure 2.10 it can be seen that the VSWR bandwidth increases for greater thickness.

2.5 Radiation pattern of the microstrip antenna

The setup for measuring the power pattern consists of a X-band horn antenna fed by a microwave source. Refer to figure 2.21. This transmitting antenna is mounted on a stand. The microstrip antenna is also mounted on a stand and acts as a receiving

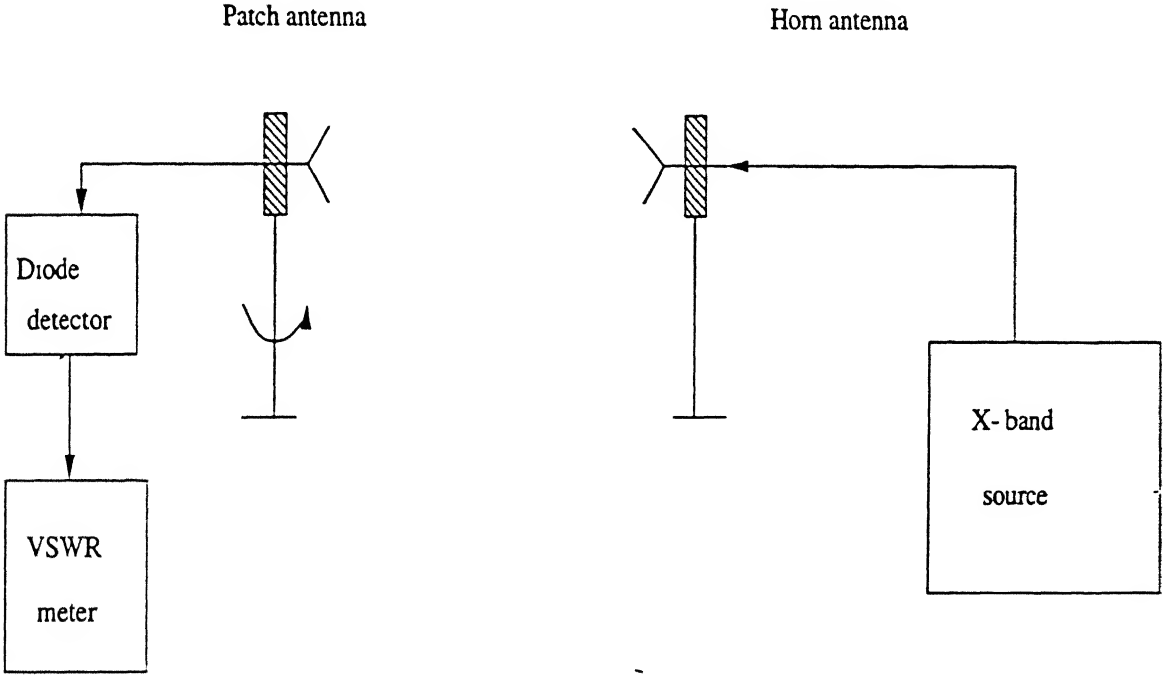

Figure 2.21: Set up for measuring radiation pattern

antenna. The output terminal of the receiving antenna is connected to a diode detector and then to a VSWR meter. The receiving antenna is rotated about the axis and received relative power is measured.

The radiation pattern was measured using the setup described earlier. The measurements were carried out in two planes.

1. $\phi = 0^o$ and radiation pattern as function of θ. Radiation pattern in H-plane is shown in the figure 2.22. The measured 3 dB bandwidth is 76^o.

2. $\phi = 90^o$ and radiation pattern as function of θ. Radiation pattern in E-plane is shown in figure 2.23. The measured 3 dB bandwidth is 90^o

According to the cavity model, the radiation pattern of the patch antenna should correspond to that of two slots separated by a distance less than $\lambda/2$. The measured radiation pattern agrees with the theory.

The radiation pattern measurements were made inside the laboratory using a X-band horn antenna as a transmitter. This measurement is not very accurate due to reflections from the walls and from other metallic instruments.

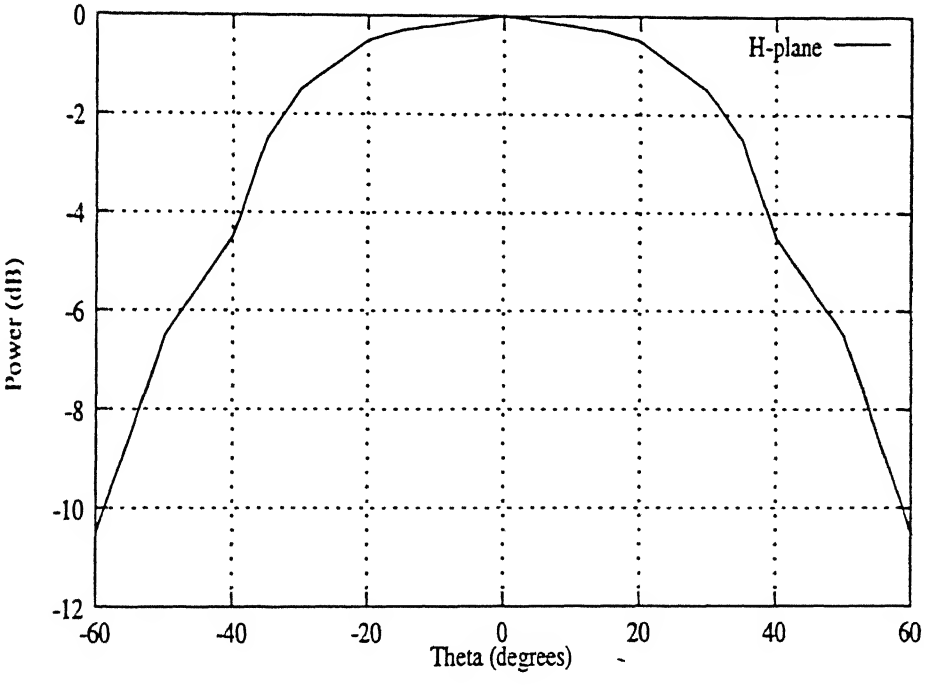

Figure 2.22: Radiation pattern in H-plane

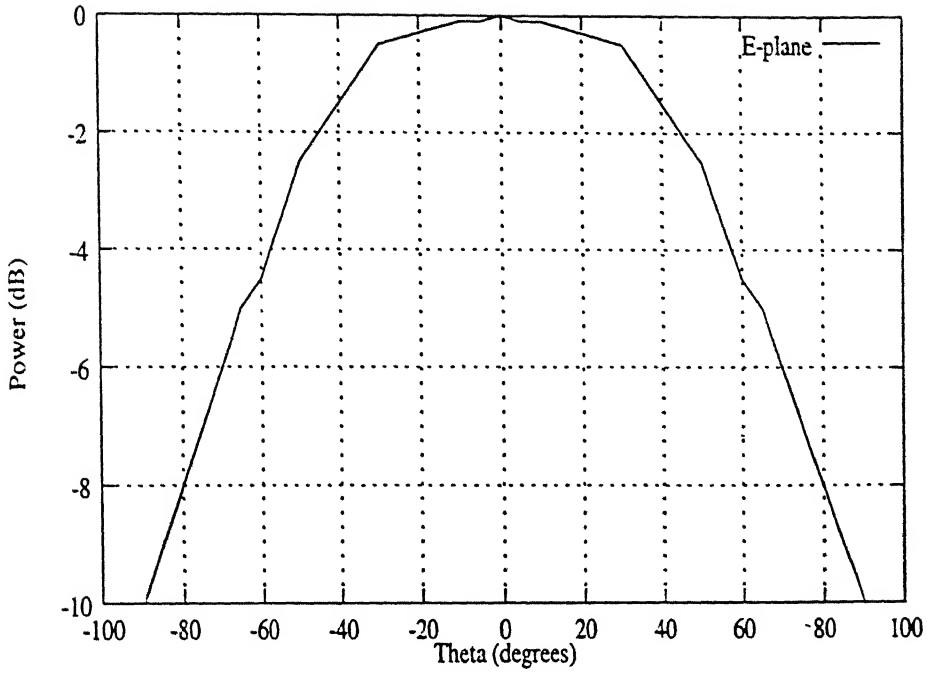

Figure 2.23: Radiation pattern in E-plane

2.6 Design procedure

This section describes the procedure to be adopted to design a EM coupled rectangular patch antenna for the required specifications. As described earlier the EM coupled rectangular patch antenna differs from the directly coupled rectangular patch antenna due to the presence of air dielectric discontinuity. The relations available for the directly coupled patch antenna and as described were used as a guideline for selecting the dimensions. The formulas available for the direct coupled patch antenna were modified accordingly.

The modified formula for finding the end correction ,Δl, is given by

$$\Delta l = .3036h' \left(\frac{\epsilon_{eff}+.3}{\epsilon_{eff}-.258}\right)\left(\frac{b/h'+.262}{b/h'+.813}\right)$$

b is the breadth of the patch, h is the height of the patch and $h' = h/2$. The effective dielectric constant ϵ_{eff} is given by

$$\epsilon_{eff} = \left(\frac{\epsilon_r+1}{2}\right) + \left(\frac{\epsilon_r-1}{2}\right)\left(1+\frac{10h}{b}\right)^{-1/2}$$

The corrected resonant frequency in GHz is given by

$$f = \left(\frac{10.103}{a+2\Delta l}\right)$$

here a is the length of the patch and $2\Delta l$ is the end correction for the two sides in cm.

Patch antenna in figure	Measured resonant frequency (GHz)	Computed resonant frequency (GHz)	Percentage error
2.13	9.78	9.89	1.12
2.14	10.35	10.4	0.48
2.15	10.65	10.7	0.47
2.16	10.9	11.0	0.92
2.17	10.4	10.6	1.92

Figure 2.24: Measured and computed resonant frequencies

Figure 2.24 gives the comparison of the measured and computed resonant frequencies of the EM coupled patch antenna. As can be seen from the table that the computed resonant frequency is in agreement with the measured value and the maximum error in percent is 1.92.

The air dielectric discontinuity in our problem behaves as an impedance transformer and thus lowers the effective input impedance. To find this transformation ratio the results of patch three were utilized. The input impedance of the directly coupled patch antenna of same dimensions were calculated using the formulas give in section 2.2. The mutual conductance G_m was computed using the NAG routine D01 AHF. As shown in the figure 2.25 these values were compared and transformation ratio was calculated for each case.

The proposed transmission line model of rectangular patch antenna (EM coupled

S.no	Computed Z_{in} for directly coupled patch (ohms)	Measured Z_{in} for EM copled patch (ohms)	width (cm)	Transformation ratio obtained
1	441.48	93.24	0.5	4.73 : 1
2	350.96	83.46	0.61	4.20 : 1
3	297.88	73.82	0.71	4.03 : 1
4	248.24	64.10	0.86	3.87 : 1
5	164.28	42.44	1.11	3.87 : 1
6	138.08	39.44	1.27	3.50 : 1

Figure 2.25: Input impedance of direct coupled and EM coupled patch antenna

is shown in the figure 2.26. Here the average transformation ratio is taken as 4:1.

It is found out that $Z_{in}/Z'_{inth} = (h/h_1)^2$

Where Z'_{inth} is the input impedance of the EM coupled patch antenna.
This is a approximate model and has been verified for h_1 equal to h_2 and ϵ_{r1} equal to ϵ_{r2}.

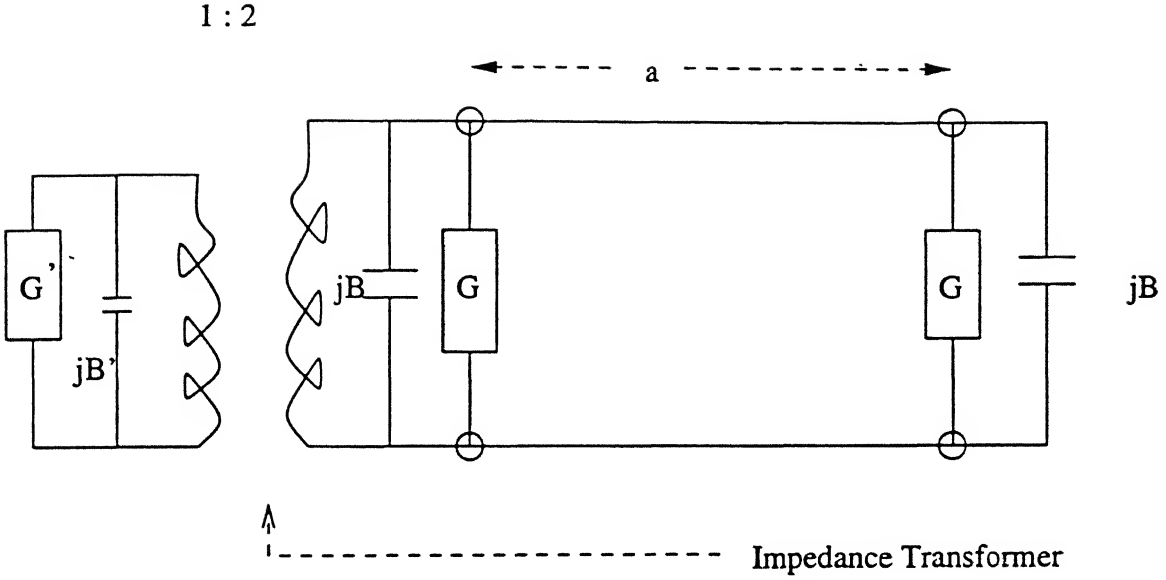

Here,

G' is the total conductance for the EM coupled patch antenna.

B' is the suceptance for the EM coupled patch antenna

Figure 2.26: The proposed transmission line model

Chapter 3

Linear Array Design

When larger directivity is required than can be obtained by a single antenna, antenna arrays are used. An antenna array is a system of similar antennas, similarly oriented. Antenna arrays make use of wave-interference phenomena that occur between the radiations from different elements of the array. An array is linear when the elements of the array are spaced equally along a straight line. The relative physical positioning of the elements and their relative electrical excitations are two parameters that can be used to exercise control over the shape of radiation pattern of an array.

To test the design of the EM coupled patch antenna and its suitability for array application it was decided to make an eight element broad side array with side lobe level below 25 dB and operating at 9.25 GHz. Taylor pattern synthesis was used to calculate relative electrical excitation of the eight elements. The spacing between the elements was chosen as 0.6 λ (here λ is the operating wavelength) so that the main lobe is covered only once thus avoiding the grating lobes. It also ensures that slight variation in λ due to change in operating frequency does not include the grating lobe. The aim here was to design a linear array antenna using the theory developed in Chapter 2. Software package LAARAN was used to calculate relative electrical excitation of the eight elements.

To design a linear array it is necessary to investigate mutual impedance between antennas. When two or more antennas are used in an array, the driving-point impedance of

each antenna depends upon the self-impedance of that antenna and in addition upon the mutual impedance between the given antenna and each of others. Theoretical analysis of the mutual impedance between rectangular patch antennas is extremely difficult and hence the necessary data has been obtained experimentally.

The corporate or parallel feed system has been used to maintain equal path lengths from the input to output ports The corporate or parallel feed system is simply a device that splits power between n output ports with a prescribed distribution while maintaining equal path lengths from the input to output port.

3.1 Mutual impedance

In the design of an array, it is important to estimate the mutual coupling between the antenna elements. Mutual coupling is caused by the simultaneous effect of interaction through surface waves, between the various elements of the array.

The S matrix approach was used to determine the mutual coupling between the array elements. This required the measurement of S_{11}, S_{12}, S_{21} and S_{22}. The measurements were done on the network analyzer (HP 8720c). 2-port calibration was performed using the TRL technique.

The setup for measuring the mutual-impedance between two rectangular patch antenna is shown in the figure 3.1. Since it was required to design a linear array antenna at 9.25 GHz design procedure formulated in the section 2.6 was used. Two rectangular blocks of dimensions $a = 1.04$ cm, $b = 1.22$ cm were printed on a duroid substrate with $\epsilon_r = 2.2$. The height h_1 of the substrate was taken as 0.8 mm. These two blocks were then cut in the laboratory.

Two different microstrip lines were fabricated for these two patch antennas by printing 50Ω lines on a duroid substrate with $\epsilon_r = 2.2$. The height h_2 was taken as 0.8 mm. These two microstrip lines were mounted on a common metallic plate. A slot was cut in the metallic plate so that it was possible to vary the distance d between the microstrip lines.

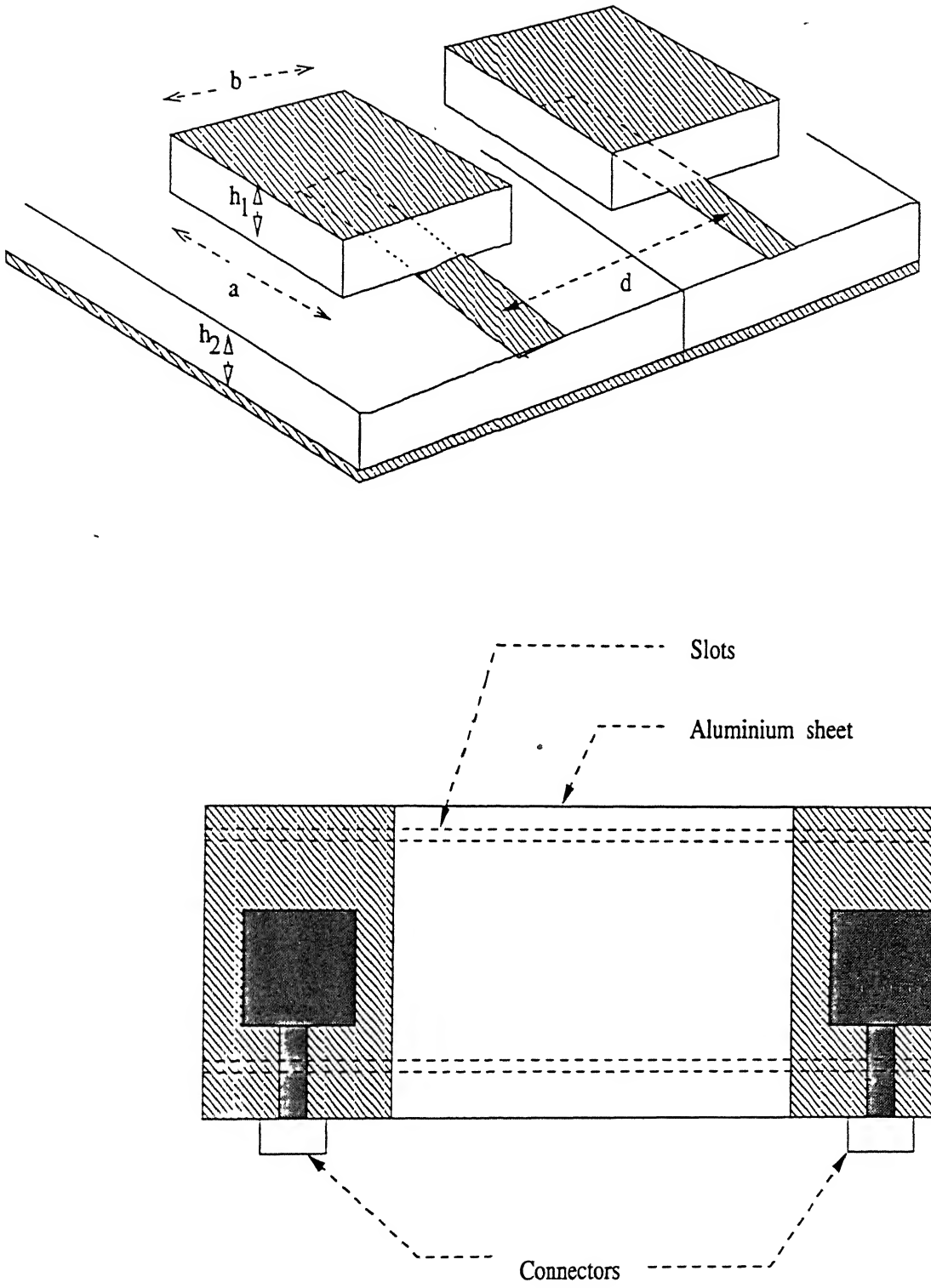

Figure 3.1: Setup for measuring mutual impedance

The two rectangular blocks were then placed symmetrically over these microstrip lines. Two connectors were then fixed at the ends of the microstrip lines. As shown in the figure distance d was varied and S-matrix was measured using the network analyzer (HP 8720c).

The S-matrix was measured at a distance of 15 mm from the connector, as established by the TRL calibration process. The correction was given in the S-matrix by multiplying the S-matrix by $e^{2j\beta l_1}$.

Here β is the propagation constant in the microstrip line and l_1 is the shift in plane of the patch antenna from the calibration plane. The mutual impedace, Z_{12}, was evaluated from the S-matrix. The mutual impedance, Z_{12}, was calculated for different d.

The variation of mutual impedance with d/λ is shown in the figure 3.2. The solid line represents the real part of the mutual impedance,R_{12}, and the dotted curve

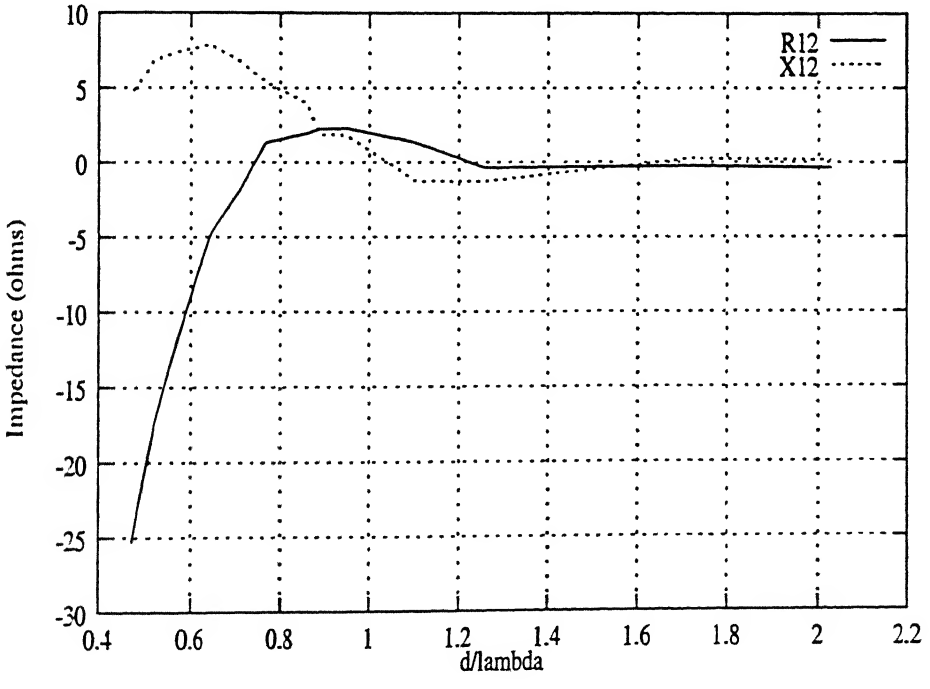

Figure 3.2: Mutual impedance vs d/lambda

represents the imaginary part of the mutual impedance,X_{12}. It can be seen from the figure that both R_{12} and X_{12} show a oscillatory behavior. The value of R_{12} and X_{12}

become negligible beyond $d/\lambda = 1.50$ and can be neglected. This figure can be utilized to calculate mutual-impedance between the elements of the linear antenna array.

3.2 Array factor design

The specification given for the linear array design were as follows :

- Center Frequency - 9.25 GHz. It was required to design the linear array which functions at 9.25 GHz.
- Band width - 0.6 GHz.
- Number of elements - 8.
- Peak side lobe level< -25 dB
- Gain - 15 dB
- The linear array antenna should have a broadside pattern.

A desirable pattern can be obtained by spacing the nulls on the appropriate arc of the unit circle. For a given width of principal lobe, the first secondary lobe can be decreased by moving the second null closer to the first. This increases the second side lobe, but that is permissible as long as it does not exceed the first. There are two ways to achieve this. the first is known as the Tchebyscheff pattern design and in this the nulls are equally spaced and the pattern is obtained with equal side lobe level. In the second, known as Taylor pattern design only the first few side lobes which are above the desired level are shifted but the remaining are unchanged. The excitation coefficients obtained by the Tchebyscheff pattern have higher excitation coefficients in the end elements and is difficult to achieve. For this reason it was decided to go for the Taylor pattern synthesis. It was also seen that if three nulls are shifted on the unit circle it is possible to obtain the desired side-lobe level, hence the number of nulls to be shifted , $\overline{n}$ was taken as three.

LAARAN software was used for calculating the array coefficients for a eight element array. The inter element spacing was taken as 0.6λ at 9.25 GHz. The side lobe level specified was -25 dB and $\overline{n} = 3$. For a Taylor pattern design, the excitation coefficients of the array were found using LAARAN which also gave the plot of distribution vs element position. Figure 3.5 gives excitation coefficients of the array as got from LAARAN.

The theoretical pattern and excitation computed by LAARAN is given in figure 3.3 and figure 3.4 respectively.

It can be seen from the figure 3.3 that the side-lobe level in the theoretical pattern given by LAARAN, all the side-lobes are below 25 dB. In the design of the array it was necessary to maintain the excitation coefficients given in the figure 3.5.

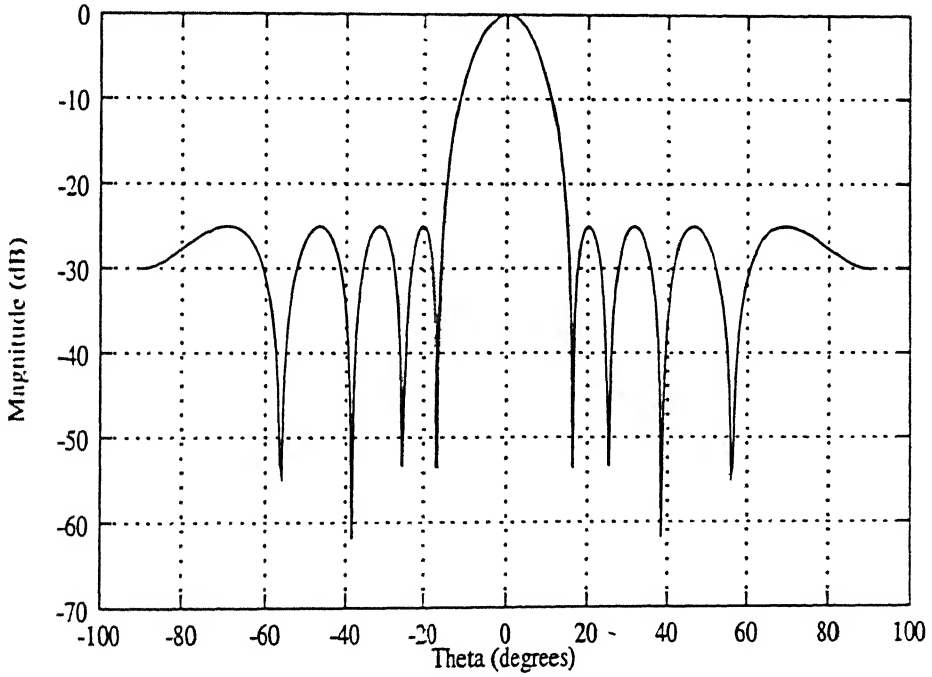

Figure 3.3: Theoretical pattern computed by LAARAN

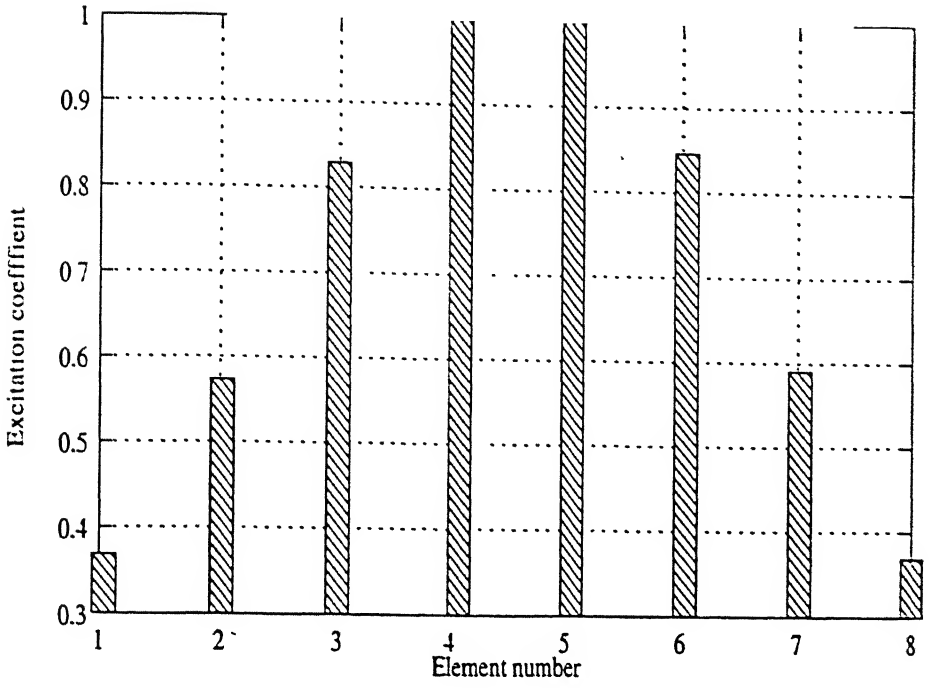

Figure 3.4: Excitation coefficients computed by LAARAN

Element	Magnitude	Phase (Degrees)
1	0.37731150	0.0000000
2	0.58430797	0.0000000
3	0.84223396	0.0000000
4	1.0	0.0000000
5	1.0	0.0000000
6	0.84223396	0.0000000
7	0.58430797	0.0000000
8	0.37731150	0.0000000

Figure 3.5: Excitation coefficients

3.3 Active impedance calculation

When two or more antennas are used in an array, the active impedance of each antenna depends upon the self-impedances of that antenna and in addition upon the mutual impedance between the given antenna and others. The feed network design of the array was to be based on the active impedance evaluated at the rectangular patch antenna element as seen by the microstrip line. The microstrip line printed at that point had to be of respective active impedance.

THE active impedance Z_m^a of the nth element can be computed using the equation:

$Z_m^a = \sum_{n=1}^{N} \left(\frac{I_n}{I_m}\right) Z_{mn}$

Here, Z_{mm} is the self impedance of the m^{th} element and Z_{mn} is the mutual impedance between the m^{th} and n^{th} element. Thus the active-impedance is the sum of of self-impedance and the current-weighted sum of the mutual impedances.
For example the active impedance, Z_1^a at the first element is given by:

$$Z_1^a = Z_{11} + rZ_{12} + r_1 Z_{13} + r_2 Z_{14} + r_3 Z_{15} + r_4 Z_{16} + r_5 Z_{17} + r_6 Z_{18}$$

Here Z_1^a is the active impedance at the first element.
Z_{11} is the self impedance of the rectangular patch antenna and is calculated from the theory developed in chapter 2.
Z_{12} to Z_{18} are the mutual impedance between the first and the second element and so on. These can be calculated using the figure 3.2.
r, r_1 to r_6 are the ratio of currents $I_2/I_1, I_3/I_1$ to I_8/I_1.
Here I_1, I_2 to I_8 are the excitation coefficients calculated from LAARAN and can be complex numbers.

In the similar way active impedances for all the eight elements were calculated. The calculated active impedances for the eight elements are given in figure 3.6.

It can be seen from the figure 3.6 that the active impedance have an imaginary part, however as seen from the figure 3.5 for a broadside pattern the excitation coefficients have to be in the same phase.
To achieve this the imaginary part of the active impedance was cancelled by vary-

S.NO.	Z^a_m	Active impedance (ohms)
1	Z^a_1	38.567 + 11.432 j
2	Z^a_2	34.235 + 16.13 j
3	Z^a_3	36.059 + 14.372 j
4	Z^a_4	36.2769 + 14.3218 j
5	Z^a_5	36.2769 + 14.3218 j
6	Z^a_6	36.059 + 14.372 j
7	Z^a_7	34.235 + 16.13 j
8	Z^a_8	38.567 + 11.432 j

Figure 3.6: Active impedance

ing the length l of the open circuit line feeding the rectangular patch antenna. The admittance of the open-circuited stub line is given by:

$$Y = j\ Y_o tan(\beta l)$$

Here Y_o is the characterstic admittance and β is the propogation constant of the microstrip line of length l. It can be seen from the figure 3.7 that this admittance of open-circuited stub line is in parallel to Y^a_m, the self admittance of the m^{th} element. The total admittance seen by the microstrip feed line at the input of the rectangular patch antenna is given by:

$$Y_{total} = Y + Y^a_m$$

It was now possible to vary the length l in such a way so as to get real value of Y_{total}. The length of the open-circuited stub line was evaluated for all the eight elements, to acheive a real value of active impedances.

The length of the stub line and the new value of active impedances for each of the eight elements is given in the figure 3.8.

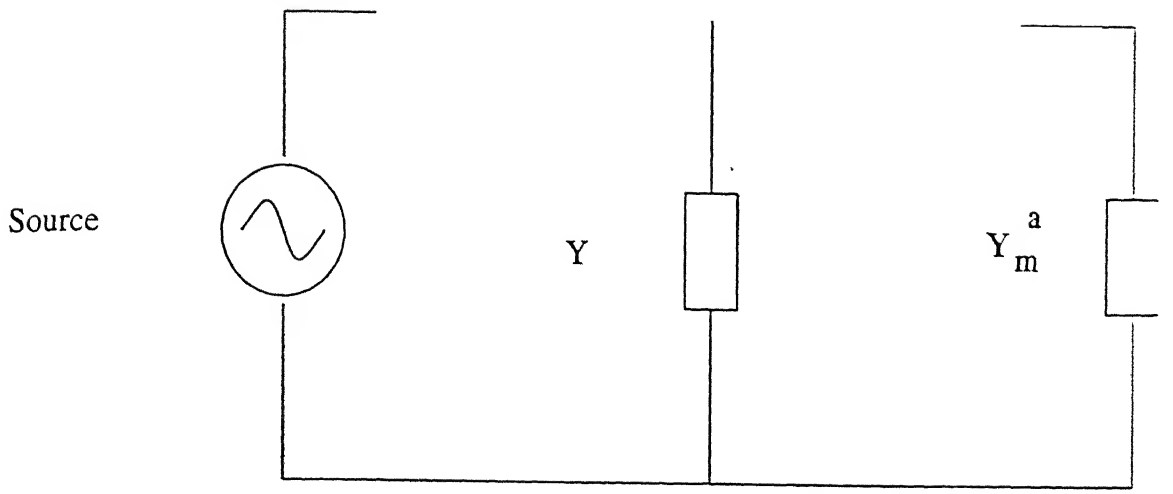

Y = Admittance of the open-circuited line of length l

Y_m^a = Active admittance of the rectangular patch antenna.

$$Y_{total} = Y + Y_m^a$$

Figure 3.7: Equivalent network of the EM coupled patch antenna

3.4 Design of feed line and power divider

The value of active impedances and the ratio of power division for each element was evaluated. The feed line structure was based on these values. There was an option between designing a corporate feed network or a serial feed network. The corporate feed network has a broader bandwidth because the phase of excitation is independent of frequency, since the path length for each line is same. On the other hand the serial feed network has a narrower bandwidth but has a lower loss. It was decided to formulate a corporate feed network for the array to cater for a wide band of operation. Power division was incorporated in the microstrip lines by making simple power dividers in microstrip line.

One example of the power divider is shown in figure 3.9. Here the power divison

Element	Stub Length(mm)	Active impedance (ohms)
1	6.88	41.95
2	6.9325	41.83
3	6.90	41.787
4	6.90	41.93
5	6.90	41.93
6	6.90	41.787
7	6.9325	41.83
8	6.88	41.95

Figure 3.8: Stub length and modified active impedance

required is 1:2. The impedance Z_1 was chosen as 50Ω. The width w_1 of the microstrip line on a duroid substrate with $\epsilon_r = 2.2$ and height $h_2 = 0.8$ mm was calculated using software package PUFF. It was required to calculate the impedances Z_2 and Z_3 at ports 2 and 3 to achieve the desired power divison.

The two simultaneous equations formed here are:

$$\frac{Z_2 Z_3}{Z_2 + Z_3} = 50$$

and

$$Z_2 + Z_3 = 200$$

Solving these two equations simultaneously, we obtain $Z_2 = Z_3 = 100\Omega$ The widths w_2 and w_3 for Z_2 and Z_3 respectively were calculated.

The widths w_2 and w_3 were gradually changed to width w_1 over a sufficient length L. The configuration of the linear patch array antenna is shown in the figure3.10.

Seven power dividers have been used in this arrangement. The feed network was printed on a duroid substrate with ϵ_r equal to 2.2. The printing was carried out in the PCB laboratory using the conventional photo-itching technique. As can be seen

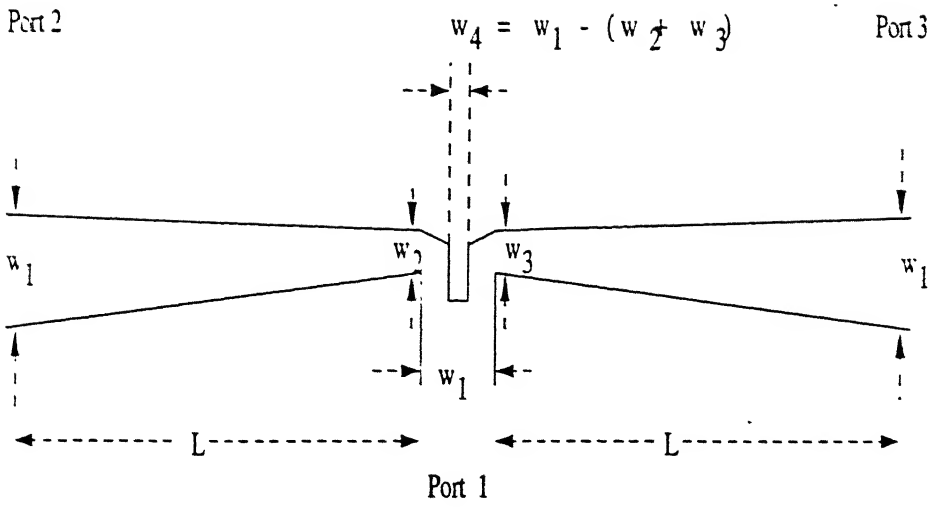

Figure 3.9: A simple power divider

from the figure that the stub length is different for all the eight elements of the array and is decided as per the data given in the figure 3.8.

GRAPHTECH CUTTING PRO was used for cutting the Rubylith sheet in the laboratory.

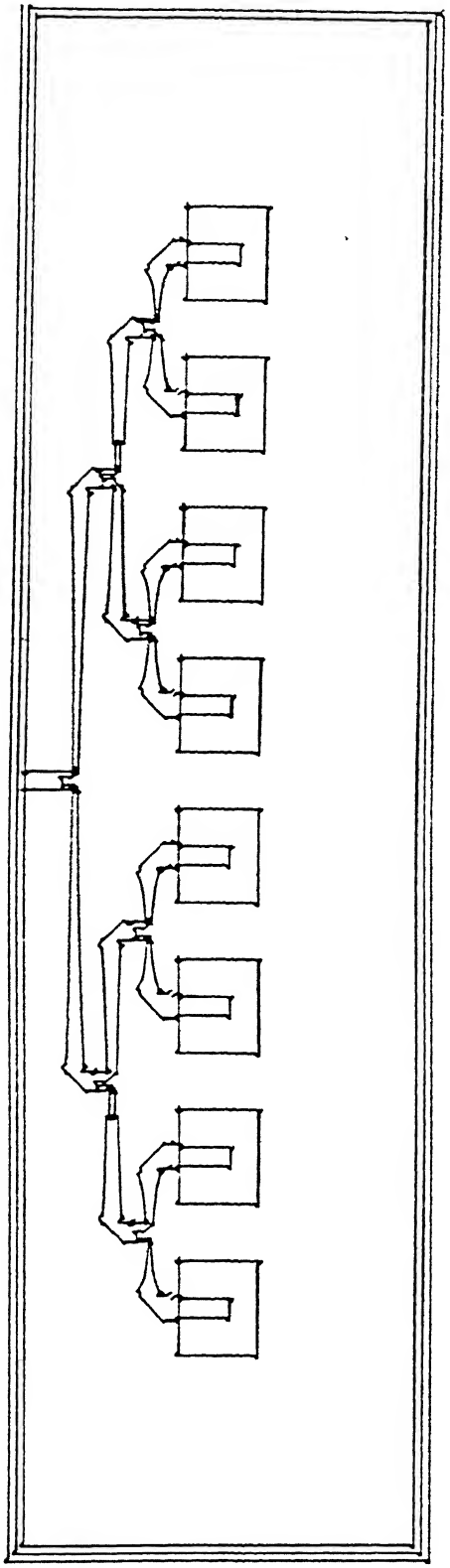

Figure 3.10: The configuration of the linear array

3.5 Fabrication and testing

The eight element rectangular patch antenna array was fabricated on a duroid substrate with $\epsilon_r = 2.2$ and $h_2 = 0.8$ mm. For ease of alignment of the rectangular patch elements a thin connection of same substrate was left. The configuration of the eight rectangular patch antennas is shown in the figure 3.11. The array was fabricated by

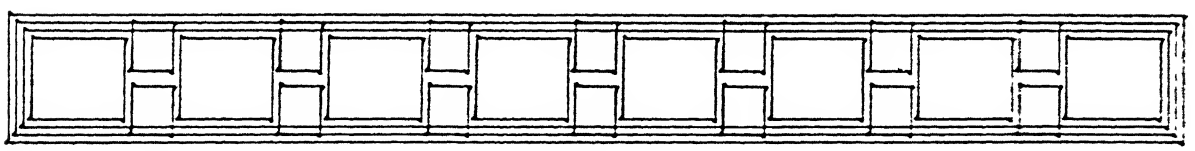

Figure 3.11: The configuration of the eight patch antennas

conventional photo-etching technique.

The measurement of S_{11} of the antenna array was performed on a network analyzer (HP 8720c). The frequeny vs magnitude S_{11} plot is given in the figure 3.12. It can be seen from the figure that the linear array antenna behaves satisfactorily in the frequency range from 9 GHz to 9.6 GHz. The minimum S_{11} of -15.5 dB is around 9.3 GHz. The antenna works over a wide band of frequencies.

The E-plane and H-plane measurement of the radiation pattern were done using the setup described in chapter 2. X-band horn antenna was used as a transmitting antenna. The H-plane pattern is given in the figure 3.13. As can be seen from the figure the minimum side lobe level is around 18 dB lower than the main lobe level. The comparison of the measured and computed pattern is given in figure 3.14.

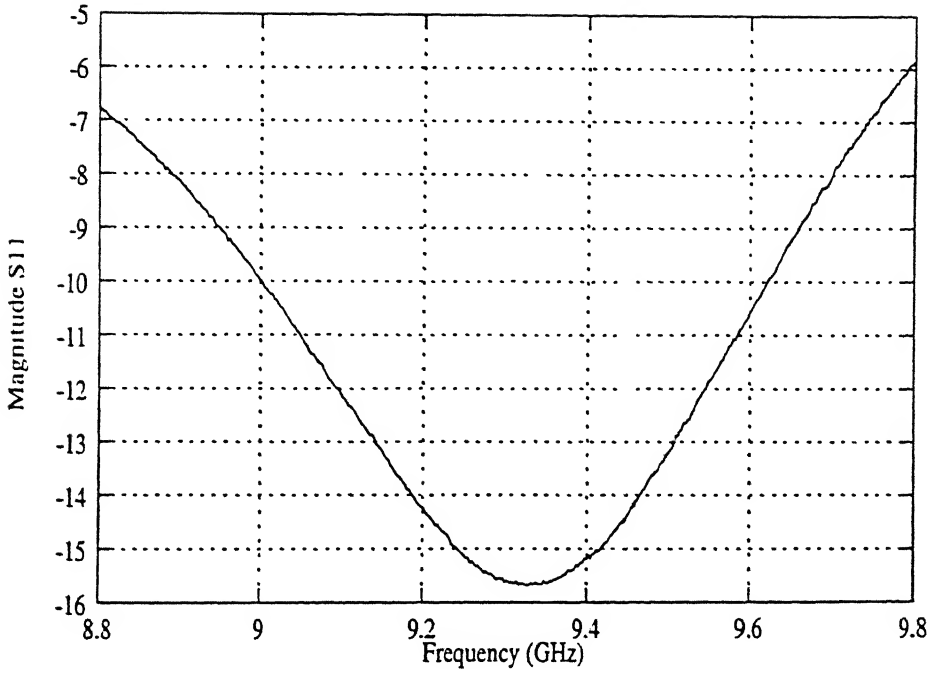

Figure 3.12: Magnitude S11 vs frequency of the linear array

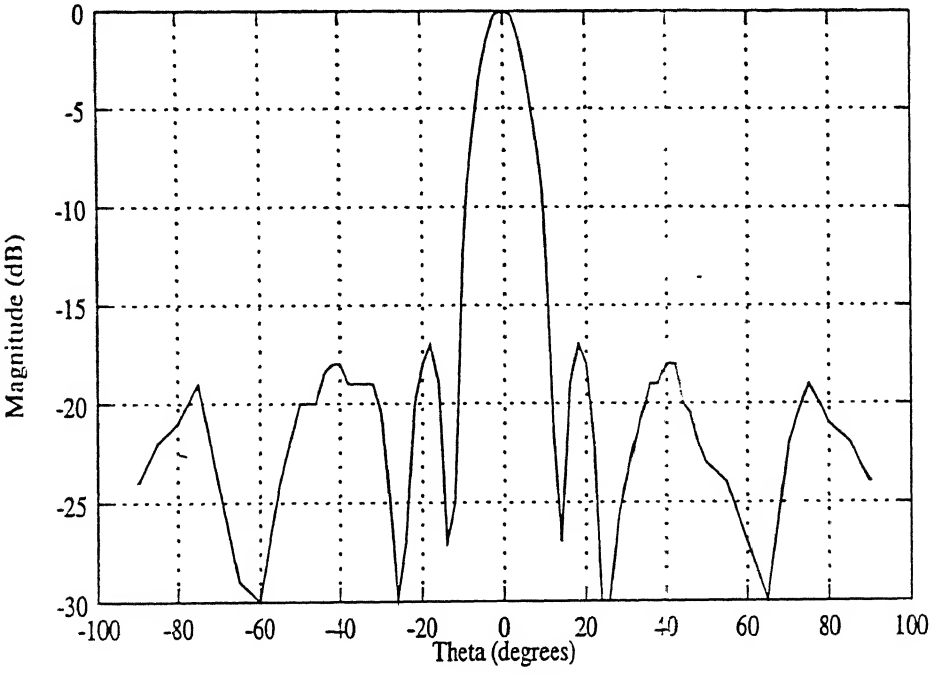

Figure 3.13: H-plane pattern of the array antenna

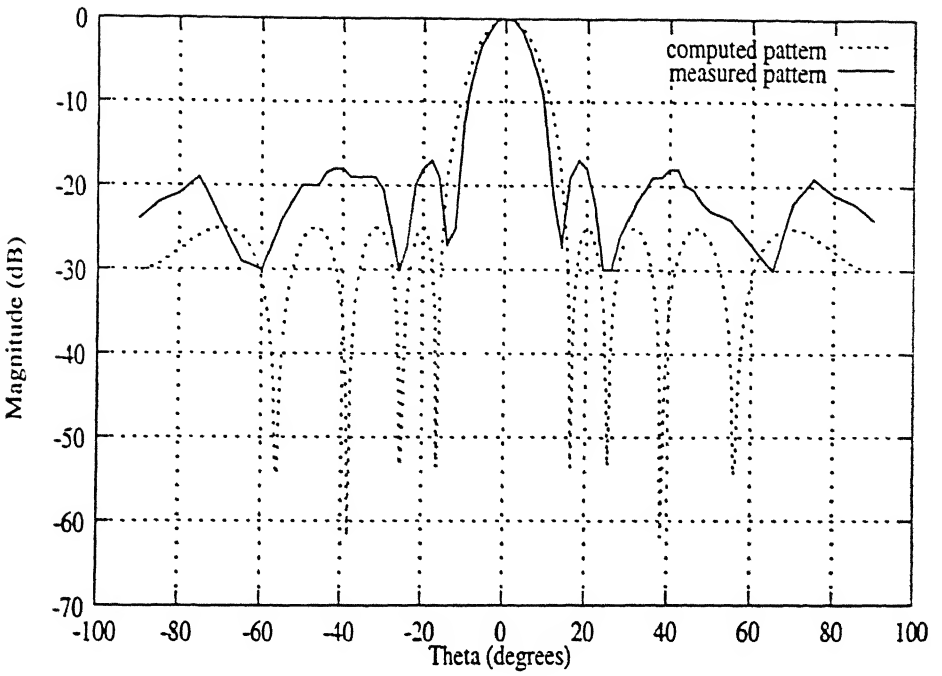

Figure 3.14: The computed and measured pattern of the linear array

The E-plane pattern is given in figure 3.15. As expected it shows a wide beamwidth. Figure 3.15 shows the plot of the co polar and cross polarization components. It can be seen from the figure that at the main lobe peak value, the cross polarization level is 35 dB lower.

The gain of the antenna was calculated using a X-band horn antenna of known gain. Initially X-band horn antenna was used as a receiving antenna and the received relative power was measured. The X-band horn antenna was then replaced by the linear array antenna and the received relative power was measured. It was observed that the gain of the array antenna was 1.6 dB lower than the X-band horn antenna. The gain of the X-band horn antenna was 15.25 dB at 9.3 GHz. Thus the gain of the linear antenna array was 13.65 dB.

The directivity of the array is evaluated using the equation:

$$Directivity = \frac{41253}{\theta_1 \varphi_1} = 16.91 dB$$

Here, θ_1 and ϕ_1 are the half power beam widths in degrees. The H-plane half power beam width is 12^o and the E-plane half power beam width is 70^o.

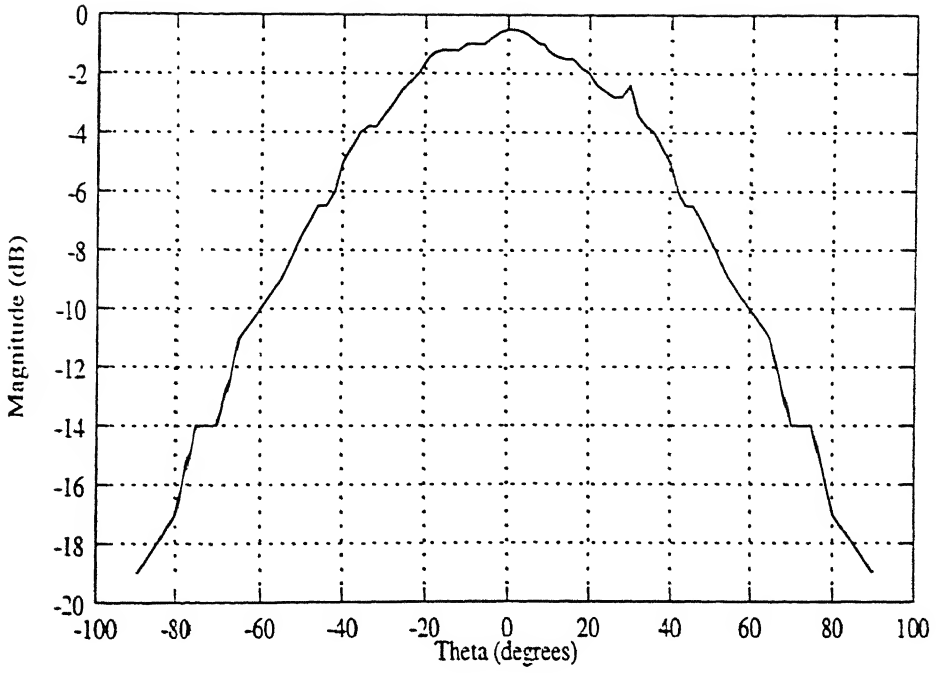

Figure 3.15: E-plane pattern of the array antenna

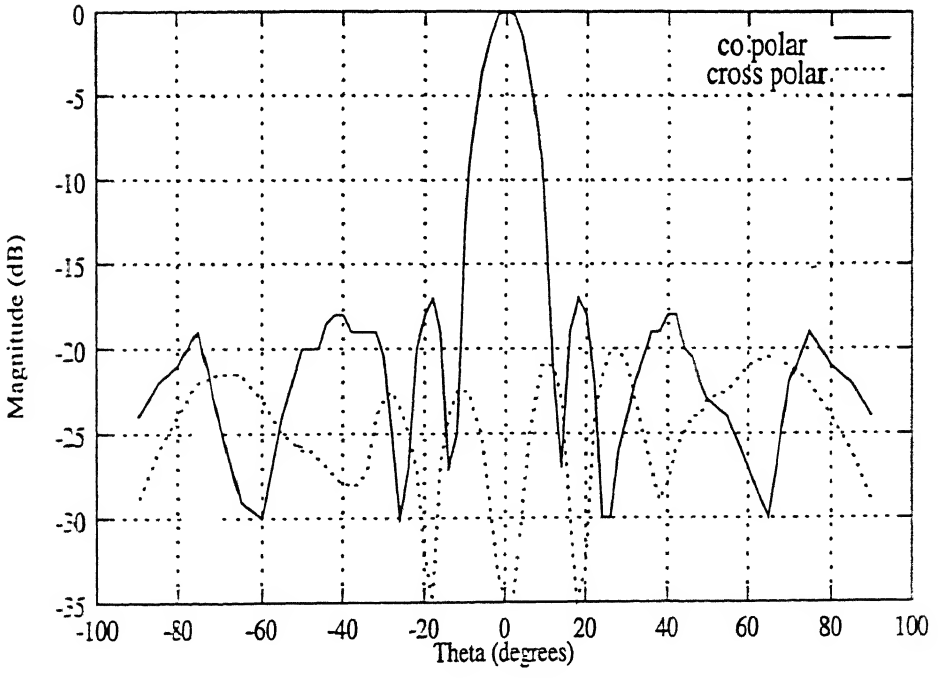

Figure 3.16: The co polar and cross polar components of the array antenna

Chapter 4

Conclusion

4.1 Summary

The microstrip antennas have notable advantages as compared to the conventional microwave antennas. The light weight, small volume and low planar configuration of the microstrip antennas has made them very popular. Narrow bandwidth is however the most significant disadvantage of the microstrip patch antennas. It is observed that the bandwidth of the microstrip antenna is a function of the height h of the dielectric substrate. The bandwidth increases considerably by using a thicker substrate. The thicker substrate however results in greater surface wave propogation leading to higher mutual coupling between the antenna array elements. The mutual coupling between the elements of an array is a function of the operating frequency and also the scan angle. The mutual coupling thus can distort the antenna pattern and hence has to be kept at the minimum. The EM coupled rectangular patch antenna is an engineering compromise between a higher bandwidth and lower mutual coupling. It utilizes the higher bandwidth of the thicker substrate but at the same time keeps the mutual coupling to the minimum.

In this study, the main objective was to study the EM coupled rectangular patch antenna. The analysis of directly coupled rectangular patch antenna was available.

The EM coupled rectangular patch antenna differs from the directly coupled patch antenna due to the presence of a air-dielectric discontinuity. This air-dielectric discontinuity makes the rigorous analysis of the EM coupled rectangular patch antenna very difficult. The approach in this study has been to carry out number of measurements on the EM coupled rectangular patch antenna and modify the available results for the directly coupled patch antenna. Network analyzer (HP 8720c) was used for measurement of S_{11} and TRL method was used for the calibration of network analyzer for better accuracy. The measurement of the antenna pattern was done in the laboratory, which is not very accurate due to the reflections from the side walls. With this the variations in the resonant frequency and input impedance with the dimensions of the rectangular patch antenna were formulated. Various design curves were also generated which can be used for fabrication of the rectangular patch antenna. The mutual coupling between the antenna elements was evaluated experimentally.

As a test of the theory developed a eight element linear array was designed and fabricated. The operating band was chosen as X-band (centre frequency 9.25 GHz). The dimensions of the rectangular patch antenna were calculated using the theory developed. The spacing between the elements was chosen as 0.6λ and the excitation coefficients required for a broadside array were calculated using the software package LAARAN. The active impedances were calculated using the mutual impedance results. The linear antenna array was fabricated using the conventional photo-itching technique on a duroid substrate with $\epsilon_r = 2.2$. Various measurements were carried out on this linear array antenna and results were in agreement of the theory.

4.2 Scope for further work

The results obtained from the study offer a lot of scope for further work. Full wave analsis of EM copled antenna will give accurate resonant frequency and input impedance. The behaviour of the EM coupled antenna for other geometrical shapes like circular, trapezoidal etc can be analysed using the cavity model and their char-

acterstics can be verified experimentally. The mutual coupling between the elements can be investigated further.

The sidelobe level of around -20 dB could be achived in the study. By ensuring more accuracy in the design and fabrication it is possible to achieve sidelobe level of -30 dB. It is also possible to achieve higher bandwidth then of 0.6 GHz as achieved in this study. The measurement of the radiation pattern was performed inside the laboratory using a very crude setup. The radiation pattern measurements can be performed in a better way.

References

[1] Deschamps, G.A., "Microstrip Microwave Antennas," presented at the 3rd USAF Symposium on Antennas, 1953.

[2] Howell, J.Q., "Microstrip Antennas," *IEEE AP-S Int. Symp. Digest*, pp. 177-180, 1972.

[3] Munson, R.E., "Conformal Microstrip Antennas and Microstrip Phased Arrays," *IEEE trans. on Antennas and Propagation*, Vol. AP-22, pp. 74-78, 1974.

[4] A.G.Derneryd, "Linearly Polarized Microstrip Antennas," *IEEE trans. on Antennas and Propagation*, Vol. AP-27, pp. 137-145, 1979.

[5] Lo, Y.T., D. Solomon and W.F. Richards, "Theory and Experiment on Microstrip Antennas," *IEEE AP-S Symposium*(Japan), pp. 53-55, 1978.

[6] Richards, W.F., Y.T.Lo and D.D.Harrison, "Improved Theory for Microstrip Antennas," *Electron. Lett.*, Vol. 15, pp. 42-44, 1979.

[7] Lo,Y.T.,D.Solomon and W.F. Richards, "Theory and Experiment on Microstrip Antennas," *IEEE Trans. on Antennas and Propagation*, Vol. AP-27, pp. 137-145, 1979.

[8] Wood, C, "Improved Bandwidth of Microstrip Antennas using Parasitic Elements," *Proc. IEEE*, Pt.H, 127, pp. 231-234, 1980.

[9] Keen, K.M, "A Planar Log-periodic Antenna," *IEEE Trans. on Antennas and Propagation*, Vol. AP-22, pp. 489-490, 1974.

[10] A.G. Derneryd, "Circular and Rectangular Microstrip Antenna Elements," *Ericsson Technics*, No. 3, 1978.

[11] A.G. Derneryd, "A Network Model of the Rectangular Microstrip Antennas," *IEEE Int. Symp. Digest*, pp.434-444, 1977.

[12] G.F. Engen, C.A. Hoer, "Thru-Reflect-Line: An improved technique for calibrating the dual six-port automatic network analyzer," *IEEE Trans. on Microwave Theory and Techniques*, December 1979.